Geophys. J. Int. (1997) **129**, 95–112

The growth of Rayleigh–Taylor-type instabilities in the lithosphere for various rheological and density structures

Clinton P. Conrad and Peter Molnar
Department of Earth, Atmospheric and Planetary Sciences, Massachusetts Institute of Technology, Cambridge, MA 02139, *USA*

Accepted 1996 November 15. Received 1996 November 1; in original form 1996 January 22

SUMMARY

Cold, dense mantle lithosphere overlying hotter, lighter, asthenosphere creates a potential instability that should be enhanced if mantle lithosphere is mechanically thickened. For timescales shorter than those during which significant heat diffuses, this instability can be treated as a Rayleigh–Taylor instability, whose basic condition consists merely of a heavy layer overlying a lighter one in a gravitational field. We have calculated growth rates of small-amplitude perturbations as a function of wavelength for several structures and boundary conditions of geological interest. In the absence of thermal diffusion, the wavelengths at which instabilities grow most rapidly are likely to be about eight times the characteristic depth scale for exponential viscosity decay, which, for typical lithosphere, yields wavelengths between 40 and 90 km. Thermal diffusion, however, smoothes out temperature-induced density perturbations and thus slows the growth of short-wavelength instabilities. As a result, wavelengths for realistic lithospheric structures are expected to increase to 100 to 200 km, with maximum values up to 300 km. As this is of the order of lithospheric thickness, a Rayleigh–Taylor instability should produce only small anomalies in topography and gravity at the Earth's surface above the downwelling. For plausible ranges of lithospheric parameters, perturbations exhibit exponential growth, with growth rates as large as 10^{-14} s^{-1}. Such rapid growth rates correspond to e-folding times of three million years, for asthenospheric viscosities of about 10^{19} Pa s. Viscosities greater than about 10^{21} Pa s allow thermal diffusion to slow growth rates to the point of stopping Rayleigh–Taylor growth completely. To simulate mechanical thickening of the lithosphere, we also include in our calculations non-zero horizontal strain rates, which can cause folding and boudinage instabilities. Folding instabilities will grow faster than those due solely to gravity when compression rates exceed about 10^{-15} to 10^{-16} s^{-1}, corresponding to shortening of 100 per cent in 30 to 300 million years. For strain rates of this magnitude, unstable growth occurs at wavelengths about 4 to 6 times the thickness of the lithosphere, as several others have previously shown. These wavelengths are significantly longer than those produced by the layered density structure alone.

Key words: Collision belts, lithosphere deformation, mantle convection, orogeny, perturbation methods, rheology.

1 INTRODUCTION

The Earth is thought to be cooling by convective heat transfer below the lithosphere and conduction of this advected heat through it. The lithosphere itself is the upper boundary layer to convection in the mantle, a fact that requires temperatures in the lithosphere to be cooler than those of the underlying mantle. These lower temperatures permit the mantle lithosphere to behave as a layer of strength, but also require densities to be greater than those of the mantle below. The resulting density inversion leads to convective downwelling of cold lithosphere into the hot mantle, manifesting itself as plate tectonics, in which lithospheric plates dive into the mantle at subduction zones. The temperature profile through the lithospheric boundary layer also creates a potentially unstable density structure within the boundary layer itself (Fig. 1). The balance between gravitational forces causing the downward flow of dense material and viscous resisting forces determines the rate at which density instabilities in the lithosphere can grow. If material can be advected in this manner faster than the perturbations can be erased by thermal diffusion, density instabilities could lead to downwelling of the lower part of the

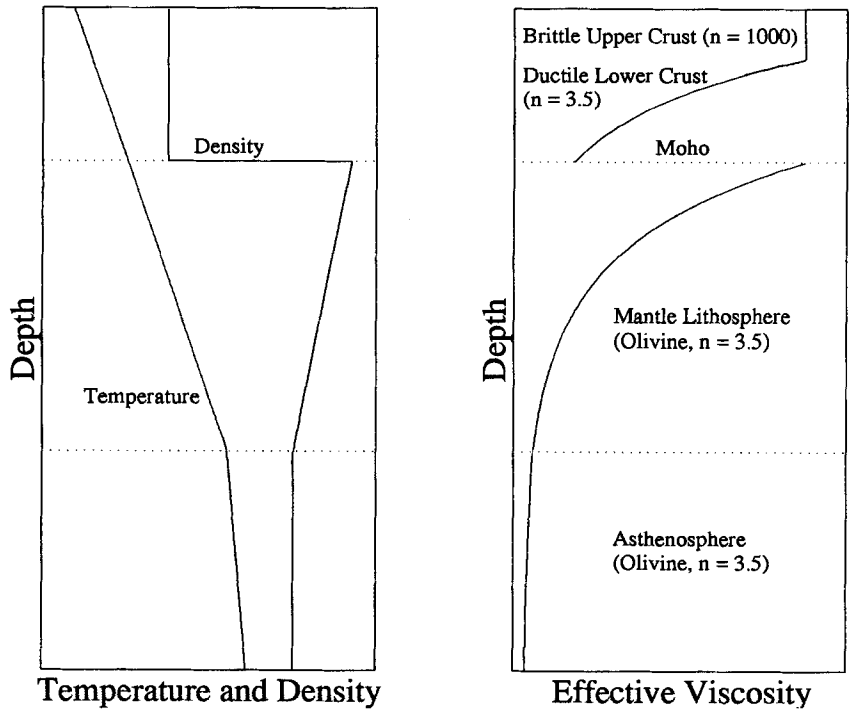

Figure 1. Cartoon of variations in temperature and density (left), and viscosity (right) through the lithosphere and into the asthenosphere.

mantle lithosphere on a horizontal scale smaller than that expected for plate tectonics.

If the lithosphere is mechanically thickened, as it could be at many mountain ranges, the density instability within the lithosphere could be enhanced. In this case, cold lithosphere will be forced downwards into hot asthenosphere, creating large lateral density gradients, which could help drive the instability (Fleitout & Froidevaux 1982; Houseman, McKenzie & Molnar 1981). Removal of the thickened lithosphere should then result in the uplift of the crustal portion of the lithosphere above (England & Houseman 1989). Because the gravitational instability produces 3-D flow, the subsequent removal of mantle lithosphere could have 3-D characteristics (e.g. Burov *et al.* 1990).

For timescales shorter than those for which heat diffusion operates, the gravitational instability at the bottom of the lithosphere can be approximated as a Rayleigh–Taylor instability. In general, the timescale for the thermal smoothing of horizontal temperature differences with wavelength λ is $\tau \approx \lambda^2/4\pi^2\kappa$, where κ is the thermal diffusivity (e.g. Turcotte & Schubert 1982, p. 154). For thermal anomalies with wavelengths, λ, between 300 and 600 km, and using $\kappa = 1$ mm^2 s^{-1}, we find $\tau = 70$ to 300 million years. Mountain belts can form on timescales shorter than this. For instance, both the Tien Shan and the Tibetan Plateau in Asia have formed since the collision of the Indian and Eurasian plates, about 50 million years ago (e.g. Molnar & Tapponnier 1975). Similarly, the crustal shortening in the Rocky Mountains of Colorado, Wyoming and Utah began between 75 and 85 million years ago and ended about 50 million years ago (Burchfiel, Cowan & Davis 1992, p. 459). For such timescales, an analysis of Rayleigh–Taylor theory can provide a simple approximation of the flow that results from the gravitational instability in the lithosphere. Moreover, simple calculations can be added to the Rayleigh–Taylor theory to approximate the retarding effect of thermal diffusion, as will be discussed later.

Lateral compression or extension of the lithosphere also causes instabilities that can grow. These instabilities result from folding or pinching of lithospheric layers, have wavelengths of the order of the thickness of the lithosphere, and grow at rates that scale with the horizontal strain rates that create them (Bassi & Bonnin 1988; Biot 1961; Fletcher & Hallet 1983; Martinod & Davy 1992, 1994; Ricard & Froidevaux 1986; Smith 1975, 1977; Zuber 1987; Zuber, Parmentier & Fletcher 1986). A few studies have included the effect of density inversions and corresponding gravitational instabilities in the lithosphere, but their analyses did not separate deformation due to gravitational instability from that due to horizontal deformation of the lithosphere (e.g. Bassi & Bonnin 1988; Ricard & Froidevaux 1986). Our goal is to isolate the effect of the gravitational instability between the lithosphere and asthenosphere. Towards this end, we focus on simple structures with density inversions to isolate the physically significant parameters and boundary conditions.

We introduce simple additions to Chandrasekhar's (1961) formalism of the infinitesimal growth of a Rayleigh–Taylor instability to study gravitational instabilities relevant to the Earth. The Earth's lithosphere is complicated by non-linear stress–strain rheology, a continuous decrease with depth of both viscosity and density, and thermal diffusion of temperature fluctuations which create density anomalies. In addition, we can include the effects of horizontal stretching or compression of the system by an external force, as presented by Bassi & Bonnin (1988), Fletcher & Hallet (1983), Ricard & Froidevaux (1986), Smith (1977), and Zuber *et al.* (1986). Some of these complications can be added to Chandrasekhar's (1961) analysis to yield analytic solutions. These analytic solutions to the Rayleigh–Taylor problem provide useful physical insight

into the behaviour of the instability. For more complex structures, we extended Bassi & Bonnin's (1988) approach to calculate growth rates numerically for various wavelengths of deformation.

2 THE DENSITY AND VISCOSITY STRUCTURE OF THE LITHOSPHERE

As previously discussed, the instability in the lithosphere arises from an increase of temperature with depth across this region (Fig. 1). This temperature gradient is approximately linear within the lithosphere, and adiabatic below it, where heat is transported largely by convection (e.g. Stacey 1992, p. 328). Continental lithosphere is thought to be roughly 100 to 300 km thick. A temperature increase of 1600 K across this region gives an average temperature gradient between 5 and 15 K km^{-1}. Ignoring pressure, the decrease of density with depth associated with temperature is (Stacey 1992, p. 250)

$$\frac{d\rho}{dz} = -\alpha_v \rho \frac{dT}{dz} . \tag{1}$$

For a density of $\rho = 3300$ kg m^{-3} and a volume expansion coefficient of $\alpha_v = 3 \times 10^{-5}$ K^{-1}, the density gradient lies between -0.5 and -1.5 kg m^{-3} km^{-1}.

Rock strength depends on temperature, so viscosity varies with depth in the lithosphere. Laboratory measurements and theory relate strain rate, ϵ, to stress difference, σ, by

$$\epsilon = A\sigma^n \exp(-E_a/RT), \tag{2}$$

where n is the power-law exponent, E_a is an activation energy, R is the gas-law constant, T is the temperature in kelvin, and A is a constant (e.g. Kohlstedt, Evans & Mackwell 1995). To convert this scalar relationship to one between tensors, one commonly exploits the second invariant of the stress tensor, which for 2-D plane strain is

$$J_2 = \frac{1}{4}(\sigma_{xx} - \sigma_{zz})^2 + \sigma_{xz}^2 . \tag{3}$$

Defining an effective viscosity, μ, in the stress–strain relationship,

$$\sigma_{ij} = 2\mu\epsilon_{ij} - p\delta_{ij} , \tag{4}$$

eq. (2) yields

$$\mu = \frac{1}{2A} \exp(E_a/RT) J_2^{(1-n)/2} , \tag{5}$$

where p is the pressure. Incompressibility requires that

$$\epsilon_{xx} + \epsilon_{zz} = 0 . \tag{6}$$

Combining (4) and (6), and assuming a pure shear field, yields

$$\sigma_{xx} - \sigma_{zz} = 4\mu\epsilon_{xx} \quad \text{and} \quad \sigma_{xz} = 0 . \tag{7}$$

Inserting these relations into (5), and solving for the viscosity gives

$$\mu = \frac{1}{2} A^{-1/n} (\epsilon_{xx})^{(1-n)/n} \exp(E_a/nRT) . \tag{8}$$

For an approximately linear geotherm through the lithosphere,

$$T(z) = T_0 - \beta z , \tag{9}$$

we can express μ as a function of z by substituting (9) into (8):

$$\mu = \mu_0 \exp(\gamma z) , \tag{10}$$

where

$$\mu_0 = \frac{1}{2} A^{-1/n} (\epsilon_{xx})^{(1-n)/n} \exp\left(\frac{E_a}{nRT_0}\right) \quad \text{and} \quad \gamma = \frac{E_a \beta}{nRT_0^2} = \frac{1}{L} , \tag{11}$$

and where we have considered a region where $T_0 \gg \beta z$. Thus, a linear increase in temperature with depth will produce an exponential decay of viscosity with characteristic decay length L (e.g. Fletcher & Hallet 1983). For an activation energy of E_a between 400 and 600 kJ mol^{-1} for olivine (Turcotte & Schubert 1982, p. 329), a temperature gradient between 5 and 15 K km^{-1}, T_0 between 1000 and 1600 K, a power-law stress–strain exponent of $n = 3.5$ (Kohlstedt *et al.* 1995), and the gas constant of $R = 8.31$ J mol^{-1} K^{-1}, L can reasonably vary between 5 and 15 km. Values of L up to about 30 km are permitted, but require extreme values of all the relevant parameters.

3 GENERAL EQUATIONS

We start by considering the general case of viscous flow, with a power-law stress–strain relationship, and depth-dependent viscosity and density, building directly on analysis developed by Chandrasekhar (1961), Fletcher & Hallet (1983), and Smith (1975, 1977). Smith (1975) showed that in their initial stages, instabilities can be treated as the growth of small perturbations to the basic background deformation. If a background flow is created by tectonic forces acting along the x-axis, they induce a horizontal strain rate, $\bar{\epsilon}_{xx}$, and a basic state of pure shear in the layered medium. Assuming plane strain and incompressibility,

$$\bar{\epsilon}_{xx} - \bar{\epsilon}_{zz} = 0 \quad \text{and} \quad \bar{\epsilon}_{xz} = 0 . \tag{12}$$

The Rayleigh–Taylor problem is a special case of the pure shear deformation in which both ϵ_{xx} and ϵ_{zz} are small; instabilities are not induced by the background flow. Some background flow is required for non-Newtonian viscosity, for if $n \neq 1$ and $\epsilon_{xx} = 0$, the viscosity as given by (8) is undefined. Thus, for non-Newtonian viscosity, some other background strain rate must be used to define the background viscosity. We can include small shear stresses in our definition of J_2, or non-zero stresses in a third dimension to do this. Alternatively, we can let $\bar{\epsilon}_{xx}$ be non-zero, but it must be small enough to prevent the development of folding or boudinage instabilities. Below, we investigate instabilities in the range of $\bar{\epsilon}_{xx}$ that represents the transition between the two types of instabilities. Henceforth, our analysis of the Rayleigh–Taylor instability for non-Newtonian viscosity implicitly assumes that some small background strain is present to define the viscosity. At a minimum, we can expect some background shear stress to be present at the top of the lithosphere due to plate motion, so we can reasonably expect the presence of some background stress with which we can define non-Newtonian viscosity.

To first order, we describe perturbations to the background stress and strain rate by

$$\tilde{\sigma}_{xx} = \frac{2\bar{\mu}}{n}\tilde{\epsilon}_{xx} - \tilde{p} , \qquad \tilde{\sigma}_{zz} = \frac{2\bar{\mu}}{n}\tilde{\epsilon}_{zz} - \tilde{p} , \qquad \tilde{\sigma}_{xz} = 2\bar{\mu}\tilde{\epsilon}_{xz} . \tag{13}$$

(Appendix A; Fletcher 1974; Fletcher & Hallet 1983; Smith 1977). Here, n is the power-law exponent, $\tilde{\sigma}$, $\tilde{\epsilon}$, and $\tilde{p}$ are first-order perturbations, denoted by a tilde, to the background

stress, strain, and pressure, denoted by an overbar. The effective viscosity, $\bar{\mu}$, can be constant or vary exponentially with depth within a layer, as in (10). For a layer of constant viscosity, we simply let L in (11) be large.

Newton's laws of motion for a continuum applied to (13) yield the Navier–Stokes equations (Fletcher & Hallet 1983):

$$\begin{aligned} 0 &= \frac{\partial \tilde{\sigma}_{xx}}{\partial x} + \frac{\partial \tilde{\sigma}_{xz}}{\partial z} \\ &= \frac{2\bar{\mu}}{n}\tilde{u}_{xx} - \tilde{p}_x + \bar{\mu}(\tilde{u}_{zz} + \tilde{w}_{xz}) + \gamma\bar{\mu}(\tilde{u}_z + \tilde{w}_x), \\ 0 &= \frac{\partial \tilde{\sigma}_{xz}}{\partial x} + \frac{\partial \tilde{\sigma}_{zz}}{\partial z} - g\tilde{\rho} \\ &= \bar{\mu}(\tilde{u}_{xz} + \tilde{w}_{xx}) + \frac{2\bar{\mu}}{n}\tilde{w}_{zz} + \frac{2\gamma\bar{\mu}}{n}\tilde{w}_z - \tilde{p}_z - g\tilde{\rho}, \end{aligned} \tag{14}$$

where subscripts now indicate partial derivatives, and we ignore inertial terms. Following Chandrasekhar (1961), we seek solutions with sinusoidal dependence on x:

$$\exp(ikx), \tag{15}$$

where k is a wavenumber. This yields

$$\begin{aligned} ik\tilde{p} &= -\frac{2\bar{\mu}}{n}k^2\tilde{u} + \bar{\mu}(D^2\tilde{u} + ikD\tilde{w}) + \gamma\bar{\mu}(D\tilde{u} + ik\tilde{w}), \\ D\tilde{p} &= \bar{\mu}(ikD\tilde{u} - k^2\tilde{w}) + \frac{2\bar{\mu}}{n}D^2\tilde{w} + \frac{2\gamma\bar{\mu}}{n}D\tilde{w} - g\tilde{\rho}, \end{aligned} \tag{16}$$

where $D = d/dz$ and variables with tildes now express only the z dependence of perturbations. The equation of continuity and the assumption of incompressibility give

$$\nabla\cdot\mathbf{u} = ik\tilde{u} + D\tilde{w} = 0, \tag{17}$$

which, when applied to (16), yields

$$\begin{aligned} k^2\tilde{p} &= -\bar{\mu}\left(\frac{2}{n} - 1\right)k^2 D\tilde{w} + \gamma\bar{\mu}(D^2 + k^2)\tilde{w}, \\ D\tilde{p} &= -\bar{\mu}(D^2 + k^2)\tilde{w} + \frac{2\bar{\mu}}{n}D^2\tilde{w} + \frac{2\gamma\bar{\mu}}{n}D\tilde{w} - g\tilde{\rho}. \end{aligned} \tag{18}$$

Eliminating pressure between these two equations yields

$$\begin{aligned} &D^4\tilde{w} + 2\gamma D^3\tilde{w} + \left(\gamma^2 - 2k^2\left(\frac{2}{n} - 1\right)\right)D^2\tilde{w} - 2\left(\frac{2}{n} - 1\right)\gamma k^2 D\tilde{w} \\ &\quad + k^2(k^2 + \gamma^2)\tilde{w} = -k^2 g\tilde{\rho}/\bar{\mu}. \end{aligned} \tag{19}$$

Conservation of mass requires

$$\frac{\partial\tilde{\rho}}{\partial t} + u\frac{\partial\bar{\rho}}{\partial x} + w\frac{\partial\bar{\rho}}{\partial z} = 0. \tag{20}$$

Allowing perturbations in density in the z-direction only, and assuming exponential growth in time with growth rate q such that $\tilde{w} \approx \exp(qt)$ gives

$$q\tilde{\rho} = -\tilde{w}\frac{d\bar{\rho}}{dz}. \tag{21}$$

Finally, applying (21) to (19) yields a homogeneous differential equation:

$$\begin{aligned} &D^4\tilde{w} + 2\gamma D^3\tilde{w} + \left(\gamma^2 - 2k^2\left(\frac{2}{n} - 1\right)\right)D^2\tilde{w} - 2\left(\frac{2}{n} - 1\right)\gamma k^2 D\tilde{w} \\ &\quad + k^2\left(k^2 + \gamma^2 - g\frac{D\bar{\rho}}{q\bar{\mu}}\right)\tilde{w} = 0. \end{aligned} \tag{22}$$

We found (22) through an analysis in two dimensions. For instabilities induced by horizontal strain rates, a 2-D analysis is appropriate because the orientation of compression or extension dictates the alignment of these instabilities. Structures that deform by a Rayleigh–Taylor instability, however, have no preferred orientation, and a 3-D analysis in required. Following Chandrasekhar (1961, p. 430), two horizontal dimensions can be combined using $k^2 = k_x^2 + k_y^2$ and a 3-D variation of (17), allowing (22) to be applied in three dimensions, but only for $n = 1$. For the general case, we use (22) to provide a solution in two dimensions, remembering that density instabilities can grow in three dimensions. We show below that the inclusion of non-Newtonian viscosity does not significantly affect the wavelength of maximum growth rate, suggesting that our analysis may be approximately valid in three dimensions for $n \neq 1$.

4 BOUNDARY CONDITIONS

The four boundary conditions are continuity of vertical and horizontal velocity and of shear and normal stress on perturbed interfaces. For a layer over a half-space, we apply two of four boundary conditions at the top, at $z = h$, and all four at the interface between them, $z = 0$. For a rigid upper boundary, the boundary conditions for vertical velocity, w, are

$$\tilde{w}_1 = 0 \quad \text{at } z = h, \quad \text{and} \quad \tilde{w}_1 = \tilde{w}_2 \quad \text{at } z = 0, \tag{23}$$

where the subscripts 1 and 2 refer to the upper and lower layers, respectively. Using (17), the continuity of u across the boundary gives

$$D\tilde{w}_1 = 0 \quad \text{at } z = h, \quad \text{and} \quad D\tilde{w}_1 = D\tilde{w}_2 \quad \text{at } z = 0. \tag{24}$$

At the interface between the two fluids, $z = 0$, small perturbations to the flow can be described by a sinusoidal variation in the z-coordinate of the boundary: $\eta \approx \cos(kx)$. Ricard & Froidevaux (1986) show that, to first order, continuity of shear stresses across a perturbed boundary requires (see Appendix B)

$$\tilde{\sigma}_{1,xz} - \tilde{\sigma}_{2,xz} = 4\bar{\epsilon}_{xx}\frac{\partial\eta}{\partial x}(\bar{\mu}_1 - \bar{\mu}_2) \quad \text{at } z = 0, \tag{25}$$

where the notation $1, xz$ denotes the shear stress in layer 1. Chandrasekhar (1961, p. 432) shows that $\tilde{\sigma}_{xz}$ can be determined from (13) and (17):

$$\tilde{\sigma}_{xz} = -\frac{\bar{\mu}}{k}(D^2 + k^2)\tilde{w}. \tag{26}$$

If viscosity is continuous across the boundary, or if the horizontal strain rate is zero, then the right-hand side of (25) is zero. As this is the only place in which $\bar{\epsilon}_{xx}$ appears, horizontal shortening can cause an instability only where there is a discontinuity in viscosity at a boundary. On the other hand, the analysis of the density instability to follow requires (25) to be homogeneous. Because non-Newtonian viscosity is only defined if there is some background stress, if $n \neq 1$ and $\bar{\mu}_1 \neq \bar{\mu}_2$, we require that this background stress be either shear stress or horizontal stress in a third dimension. Non-zero values of $\bar{\epsilon}_{xx}$ do not provide a homogeneous boundary condition.

Finally, continuity of normal stress, σ_{zz}, is perturbed by the displacement of the interface between two layers of different density (see Appendix B):

$$\tilde{\sigma}_{1,zz} - \tilde{\sigma}_{2,zz} = (\rho_2 - \rho_1)g\eta \quad \text{at } z = 0. \tag{27}$$

If $\rho_1 > \rho_2$, this boundary condition generates a gravitational instability. Using (13) to determine $\tilde{\sigma}_{zz}$, and eliminating $\tilde{p}$ using (18), we obtain

$$\tilde{\sigma}_{zz} = \bar{\mu}\left[-\frac{1}{k^2}D^3 - \frac{\gamma}{k^2}D^2 + \left(\frac{4}{n}-1\right)D - \gamma\right]\tilde{w}. \tag{28}$$

We may eliminate η in (27) by taking its time derivative, which is the vertical velocity, $\tilde{w}$. If, as assumed before, $\tilde{w}$ grows exponentially, (28) becomes

$$\left[-D^3 - \gamma D^2 - \left(\frac{4}{n}-1\right)k^2 D - k^2\gamma\right](\bar{\mu}_1\tilde{w}_1 - \bar{\mu}_2\tilde{w}_2)$$
$$+(\rho_1-\rho_2)gk^2\tilde{w}_1/q = 0. \tag{29}$$

As (22) is a fourth-order differential equation, a complete description of flow in each layer requires four eigenfunctions with four undetermined coefficients. The lower half-space requires only two, as its flow must not diverge at depth. Thus, for m layers (including the half-space), we seek $4m+2$ unknowns, determined by $4m+2$ boundary conditions.

5 ANALYTIC SOLUTIONS

For cases in which the background strain rate, $\bar{\epsilon}_{xx}$, is zero (i.e. the Rayleigh–Taylor case), we can find analytic solutions to (22), following the approach of Bassi & Bonnin (1988), Chandrasekhar (1961), and Whitehead & Luther (1975), of the form

$$\tilde{w} = \exp(ksz + qt), \tag{30}$$

where $s = \alpha + \beta i$. The constants α and β are given by Bassi & Bonnin (1988) and in Appendix C. For the case of a layer over a half-space, with a rigid upper boundary, boundary conditions (23), (24), (25), and (29) provide six equations and six unknowns. For cases in which $\bar{\epsilon}_{xx} = 0$, and background viscosities are properly defined, the right-hand sides of all six boundary conditions are zero. In matrix form:

$$\mathbf{MC} = 0 \tag{31}$$

where $\mathbf{M}$ is a 6×6 matrix containing the six boundary conditions, and $\mathbf{C}$ is a vector containing the six undetermined coefficients. We simplify the elements of $\mathbf{M}$ by non-dimensionalizing the wavenumber, k, and growth rate, q, by the relevant length- and time-scales. For the case of a layer over a half-space with constant viscosity in both, we use

$$q = \frac{(\rho_1-\rho_2)gh}{\mu_1}q' \quad \text{and} \quad k' = kh, \tag{32}$$

where q' and k' are the dimensionless growth rate and wavenumber.

For a non-trivial solution for $\mathbf{C}$, $\mathbf{M}$ must have a non-trivial nullspace, which implies that the determinant of $\mathbf{M}$ must be zero. Setting $\det(\mathbf{M}) = 0$ yields an equation relating q', k', and n. We used a symbolic mathematical manipulation program, MAPLE, to alleviate the tedium of calculating this solution. The function $q'(k')$ generally has a maximum at a unique wavenumber $k'_{\max}$: $q'_{\max} = q'(k'_{\max})$. Because the growth rate for $k'_{\max}$ is largest, perturbations with this wavenumber will grow most rapidly. If we assume that the interface is initially perturbed at all wavenumbers, then the flow will be dominated, at least at small amplitudes, by deformation with wavenumber $k'_{\max}$. We have calculated $k'_{\max}$ and $q'_{\max}$ for various boundary conditions and viscosity and density structures.

5.1 Layer over a half-space

First, we consider a layer of thickness h overlying a half-space with ρ and μ constant in each. Thus, $L\to\infty$, or $\gamma = 0$. The ratio of the viscosity of the top layer to that of the lower half-space is given by the constant $r = \mu_1/\mu_2$. For the same exponent, n, describing power-law creep in both layers, the solution to $\det(\mathbf{M}) = 0$ gives

$$q' = \left(\frac{r}{2b}\right)\frac{(n-1)[r\sinh(2b)+\cosh(2b)] + 2\cos^2(c) - r\sqrt{n-1}\sin(2c) - n - 1}{(n-1)[(r^2+1)\cosh(2b) + 2r\sinh(2b)] - (r^2-1)[2\cos^2(c) - n - 1]}, \tag{33}$$

where

$$b = \frac{k'}{\sqrt{n}} \quad \text{and} \quad c = \frac{k'\sqrt{n-1}}{\sqrt{n}}. \tag{34}$$

For $\mu_1 = \mu_2$ giving $r = 1$, (33) simplifies to

$$q' = \frac{2(n-1)\sinh(b)\exp(b) - \sqrt{n-1}\sin(2c) - 2\sin^2(c)}{4b(n-1)[\sinh(2b) + \cosh(2b)]} \tag{35}$$

plotted in Fig. 2(a). If $n = 1$, for Newtonian viscosity, (35) simplifies to

$$q' = \frac{1 - (2k'^2 + 2k' + 1)\exp(-2k')}{4k'}, \tag{36}$$

for which $q'_{\max} = 0.097$ occurs at $k'_{\max} = 1.69$, or $\lambda_{\max} = 3.7h$. If $n = \infty$, corresponding to a purely plastic medium, (35) simplifies to

$$q' = \frac{k' - \sin(k')\cos(k')}{2k'}, \tag{37}$$

which reaches a maximum where $\tan(2k') = 2k'$, giving $q'_{\max} = 0.61$ at $k'_{\max} = 2.25$, or $\lambda_{\max} = 2.8h$. As shown in Fig. 2(a), there are several maxima, at approximately even intervals of $\Delta k' = \pi$, the amplitudes of which decrease as k' increases. Whereas $q'_{\max}$ increases monotonically with n, $k'_{\max}$ does so only slightly (Fig. 3).

Suppose instead that the viscosity of the upper layer is much larger than that of the lower layer. For $\mu_1 \gg \mu_2$, giving $r\to\infty$, (33) simplifies to

$$q' = \frac{\sqrt{n}\sqrt{n-1}}{4k'}\left(\frac{\sqrt{n-1}\sinh(2b) - \sin(2c)}{(n-1)\cosh^2(b) + \sin^2(c)}\right) \tag{38}$$

(Fig. 2b). Again we look at two special cases. For $n = 1$, (38) reduces to

$$q' = \frac{1}{2k'}\left(\frac{\cosh(k')\sinh(k') - k'}{k'^2 + \cosh^2(k')}\right), \tag{39}$$

giving $q'_{\max} = 0.16$ at $k'_{\max} = 2.12$, or $\lambda_{\max} = 3.0h$. If $n = \infty$, (38) also reduces to (37).

The special cases of $r = 1$ and $r\to\infty$ are members of a family of solutions in which we allow r to vary. For $r > 10$, $k'_{\max}$ and $q'_{\max}$ are approximately constant, indicating that (38) is approximately valid for all $r > 10$ (Fig. 4). In addition, as n increases, $k'_{\max}$ and $q'_{\max}$ become decreasingly dependent on r and approach the values given by (37).

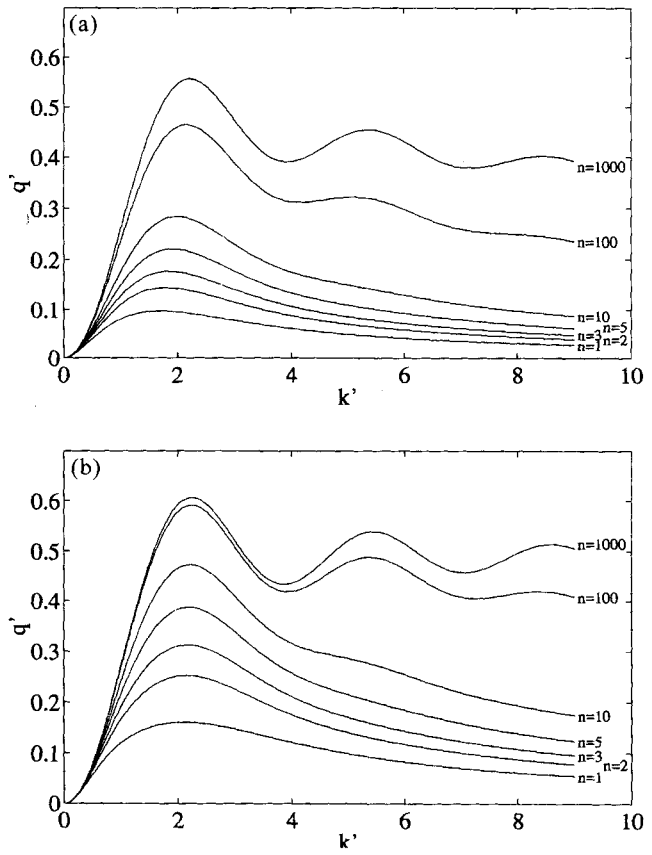

Figure 2. Dimensionless growth rate q' versus dimensionless wavenumber k' for a layer over a half-space and a rigid upper boundary, for various values of n. (a) Solutions to (35) for $\mu_1 = \mu_2$. (b) Solutions to (38) for $\mu_1 \gg \mu_2$. Non-dimensionalization is given by (32).

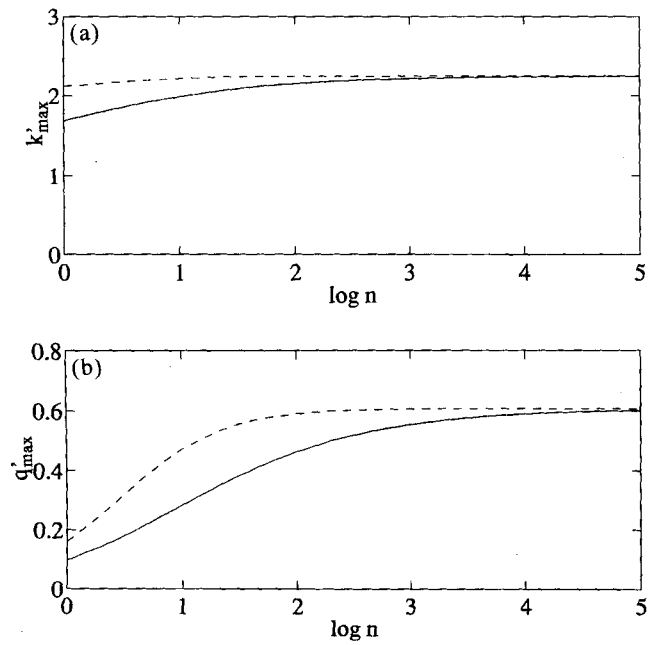

Figure 3. (a) Plot of k'_{max} versus n for a layer over a half-space. Solid line denotes curves for which $\mu_1 = \mu_2$. Dashed line represents curves in which $\mu_1 \gg \mu_2$. Non-dimensionalization is given by eq. (32). (b) Similar plot of q'_{max} versus n for the same two models.

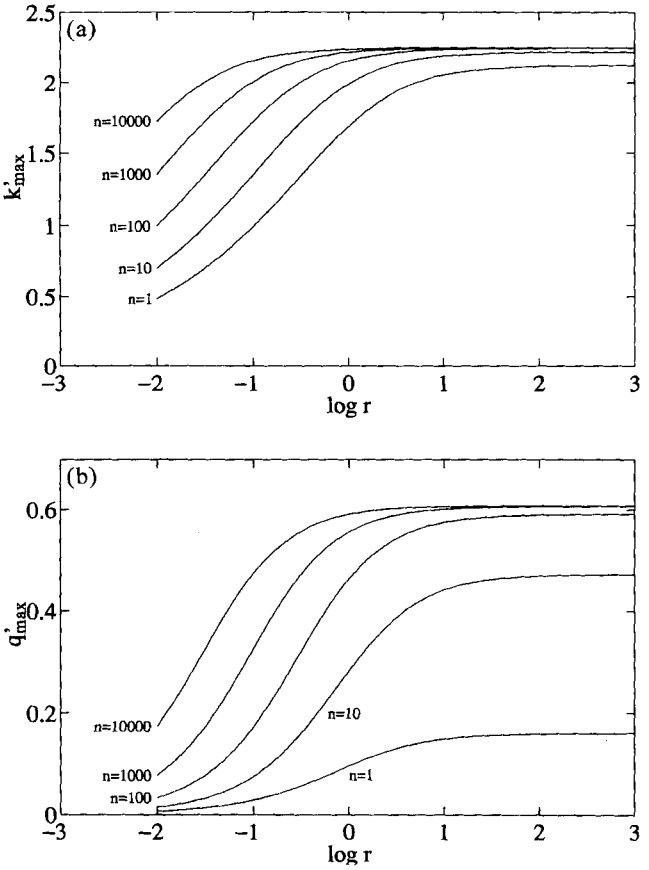

Figure 4. (a) Plot of k'_{max} versus r where $r = \mu_1/\mu_2$ for a layer over a half-space and a rigid upper boundary, for various values of the power-law exponent, n. Non-dimensionalization is by (32). (b) Similar plot of q'_{max} versus r.

5.2 Exponential decay of viscosity

The viscosity of the lower lithosphere, as discussed previously, should vary exponentially with depth. For exponentially varying viscosity, a rigid top, and a layered density structure, the growth rate depends on both L and h. To isolate a dependence on L, we consider the case of two infinite half-spaces of different densities, but with continuous viscosity across their boundary at $z = 0$. Thus, we use only four boundary conditions at the interface [eqs (C6) to (C9) of Appendix C] and disallow divergence of the solution in either half-space. We redefine the dimensionless expressions for q' and k' in terms of γ:

$$q = \frac{(\rho_1 - \rho_2)g}{\gamma \mu_1(0)} q' \quad \text{and} \quad k' = \frac{k}{\gamma} = kL. \tag{40}$$

The boundary conditions produce a 4×4 matrix **M** that must satisfy $\det(\mathbf{M}) = 0$. Solving for q' in terms of k' and the power-law exponent, n, gives

$$q' = \frac{n^2 a k'}{n^2 + 4nk'^2 - 4k'^2 + 4n^2 a^4 k'^2} \tag{41}$$

(Fig. 5), where a is given by (C2) and depends on n. For $n = 1$, (41) simplifies to

$$q' = \frac{ak'}{1 + 4a^4 k'^2} \tag{42}$$

and reaches a maximum of $q'_{max} = 0.13$ at $k'_{max} = 0.89$, or $\lambda_{max} = 7.1L$. As n increases, q'_{max} approaches 0.5 (Fig. 6), and

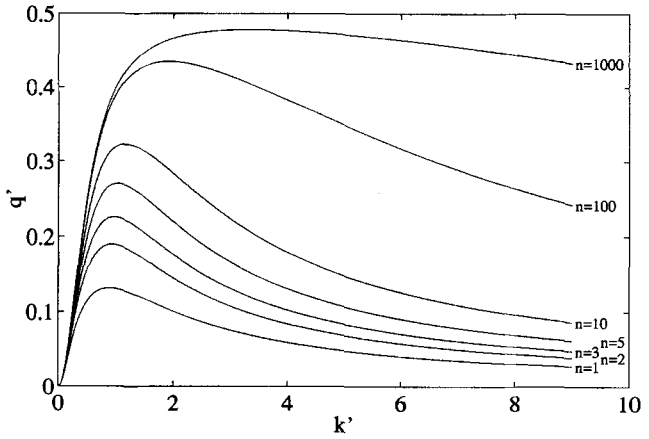

Figure 5. q' versus k' for a viscosity profile that decreases exponentially with depth as given by (41). Non-dimensionalization is by (40).

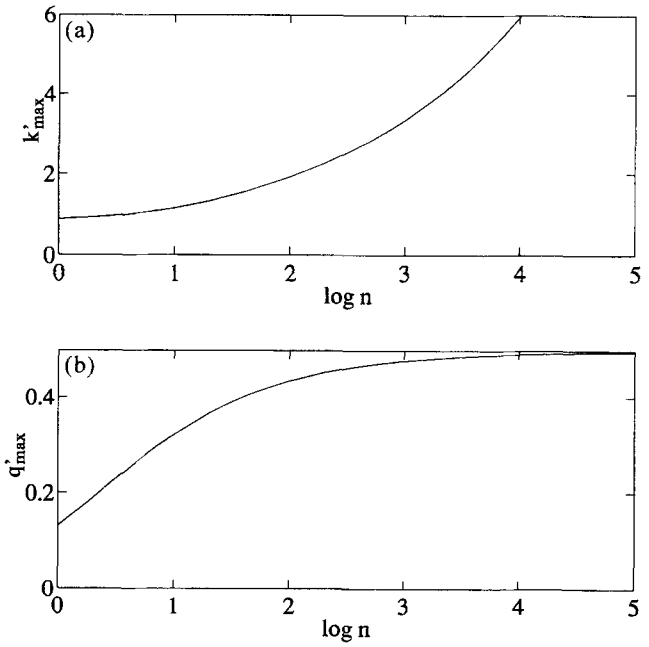

Figure 6. As Fig. 3, except for a viscosity profile that decreases exponentially with depth. Non-dimensionalization is given by (40).

for $n=\infty$, (41) becomes

$$q'=\frac{2k'^2}{1+4k'^2}, \tag{43}$$

where $q'=0.5$ as $k'\to\infty$. There is no maximum value of q', but large values of k' (small wavelengths) seem to be the preferred mode of deformation in plastic materials.

5.3 Linear decay of density

Density can be expected to decrease linearly with depth in the lithosphere. Consider a layer over a half-space in which the density decreases from ρ_1 at the top of the upper layer to ρ_2 at the bottom and is continuous across the interface, $z=0$. Here, $D\bar{\rho}=(\rho_1-\rho_2)/h$. As (22) is too complicated to be solved analytically for variable or non-Newtonian viscosity, we consider only $\gamma=0$ and $n=1$. Non-dimensionalizing by (32), (22) becomes

$$D^4\tilde{w}-2k^2D^2\tilde{w}+k^2\left(k^2-\frac{g(\rho_1-\rho_2)}{q\bar{\mu}_1 h}\right)\tilde{w}=0. \tag{44}$$

Assuming a solution of the form (30), (44) becomes

$$s^4-2s^2+1-\frac{1}{q'k'^2}=0. \tag{45}$$

Four solutions for s exist, giving four eigenfunctions for the general solution to (44):

$$W_1=A\,e^{ks_1z}+B\,e^{-ks_1z}+C\,e^{ks_2z}+D\,e^{-ks_2z}, \tag{46}$$

where

$$s_1=\sqrt{1+\delta}, \qquad s_2=\sqrt{1-\delta}, \qquad \delta=\frac{1}{k'\sqrt{q'}}. \tag{47}$$

For the 6×6 matrix, **M**, described in Appendix C, and for $\det(\mathbf{M})=0$, $\mu_1=\mu_2$ yields

$$3\delta\sinh(k's_1)\sinh(k's_2)+s_1s_2\delta[1+\cosh(k's_1)\cosh(k's_2)]$$
$$+2\delta s_2\sinh(k's_1)\cosh(k's_2)2\delta s_1\cosh(k's_1)\cosh(k's_2)=0. \tag{48}$$

The obvious solution $s_2=0$, or $q'=1/k'^2$, makes the eigenfunctions in (46) degenerate and is not physically meaningful. The next largest root of (48) dominates the growth of perturbations. We numerically solved (48) for q' as a function of k' (Fig. 7). The largest root after $q'=1/k'^2$ has a maximum of $q'_{\max}=0.037$ at $k'_{\max}=2.2$, or $\lambda_{\max}=2.9h$, compared with $q'_{\max}=0.097$ and $\lambda_{\max}=3.7h$ for a layer of constant density.

For the case in which $\mu_1\gg\mu_2$, $\det(\mathbf{M})$ yields

$$(4-3\delta^2)\sinh(k's_1)\sinh(k's_2)$$
$$-s_1s_2[(\delta^2-4)+(\delta^2+4)\sinh(k's_1)\sinh(k's_2)]=0. \tag{49}$$

Ignoring the degenerate solution $q'=1/k'^2$, $q'_{\max}=0.059$ at $k'_{\max}=2.6$, or $\lambda_{\max}=2.4h$. Again, the maximum wavelengths and growth rates are somewhat smaller than their corresponding values of $q'_{\max}=0.16$ and $\lambda_{\max}=3.0h$ for a layer of constant density.

6 EIGENVALUE APPROACH

For cases of multiple layers with attendant multiple length-scales, we must turn our analysis to numerical solutions such as those given by Bassi & Bonnin (1988). We use the solution to eq. (22) for constant density within layers in Appendix C. From this solution for $\tilde{w}$, it is easy to calculate $\tilde{u}$, $\tilde{\sigma}_{xz}$, and $\tilde{\sigma}_{zz}$ from (17), (26), and (28) and apply them to the boundary conditions (23) to (25) and (27).

These boundary conditions can be arranged in a matrix equation:

$$\mathbf{MC}=\mathbf{R}, \tag{50}$$

where **M** is a $4m+2\times4m+2$ square matrix consisting of eigenfunctions evaluated at the boundaries, **C** is a vector of undetermined coefficients, and **R** is a vector consisting of the right-hand sides of the boundary conditions. The right-hand sides of (25) and (27) allow the inclusion of perturbations due to both gravity and horizontal strain rate, $\bar{\epsilon}_{xx}$. We define the amplitude, η_i, of a perturbation to each interface i, using a

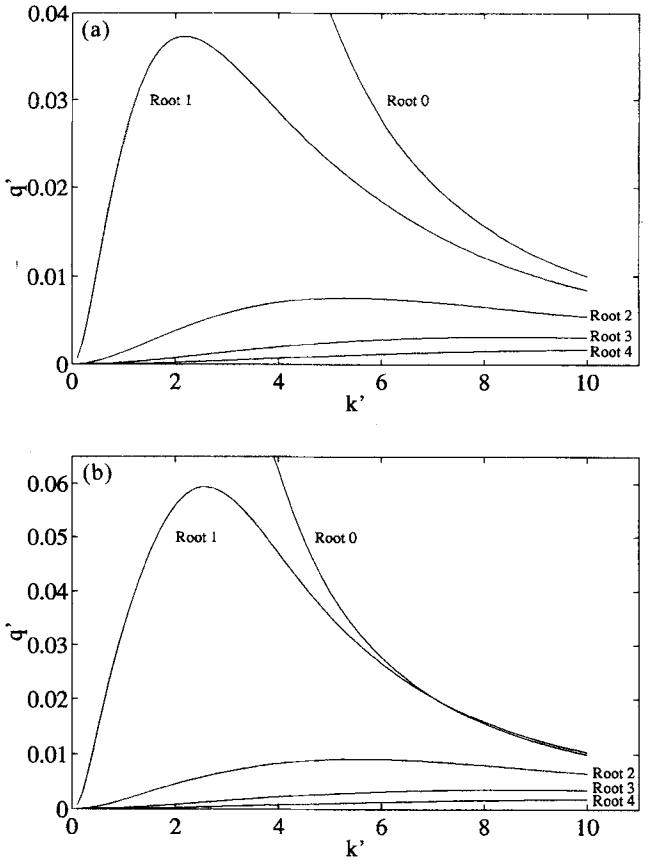

Figure 7. (a) Plot of q' versus k' for a linear decay of density with depth and $\mu_1 = \mu_2$. The curve labelled 'Root 0' represents a degenerate solution which results as a solution to (48) but has no physical relevance. The next largest solution, 'Root 1', is then the solution that controls the deformation. Other roots exist and are shown, but they do not contribute to the deformation because their growth rates are smaller than those of 'Root 1'. (b) Similar plot for $\mu_1 \gg \mu_2$.

vector **H**:

$$\mathbf{H}(t) = \sum_{i=1}^{m} \eta_{i0} \mathbf{V}_j \, e^{q_j t}, \tag{51}$$

where η_{i0} is the initial perturbation of each interface, $\mathbf{V}_j$ is a normalized vector consisting of the relative amplitudes of perturbations to each layer, and q_j is the corresponding growth rate; η_{i0}, $\mathbf{V}_j$, and q_j are functions of the wavenumber, k. The time derivative of the amplitude is simply the vertical velocity:

$$\mathbf{W} = \frac{d\mathbf{R}}{dt}. \tag{52}$$

However, **W** can be expressed as a linear function of **C** by

$$\mathbf{W} = \mathbf{QC}, \tag{53}$$

where **Q**, an $m \times 4m+2$ matrix, expresses this relationship.

The right-hand sides of both boundary conditions (25) and (27) are linear in η_i, if η_i is a sinusoidal function of x. Thus, **R** is a linear function of **H**:

$$\mathbf{R} = \mathbf{PH}, \tag{54}$$

where **P** is a $4m+2 \times m$ matrix. Combining (50) and (52) to (54) yields

$$\frac{d\mathbf{H}}{dt} = (\mathbf{QM}^{-1}\mathbf{P})\mathbf{H}. \tag{55}$$

This equation has the solution (51), where q_j are the eigenvalues of the matrix $\mathbf{QM}^{-1}\mathbf{P}$, and $\mathbf{V}_j$ are their corresponding eigenvectors. The largest growth rate, q, will dominate the growth of perturbations on the interface, and its corresponding eigenvector, **V**, will describe the relative amplitudes of deformation at each interface for this mode. Note, however, that in the presence of background strain, $\bar{\epsilon}_{xx}$, perturbations will grow only if their growth rates are larger than $\bar{\epsilon}_{xx}$; otherwise the background state of pure shear will overwhelm them.

6.1 Exponential decay of viscosity in a layer

As we discussed previously, the representation of the lithosphere as a layer over a half-space with exponential decay of viscosity necessitates the use of two length-scales, the viscosity decay length, L, and the thickness of the layer, h. Because the analytical solution is quite complicated, we exploit the numerical solutions described above. Let us consider a rigid upper boundary and power-law exponent, n. Fig. 8 shows how $q'_{\max}$ and $k'_{\max}$ vary with the ratio L/h for non-dimensionalization by L using (32) and for h using (40), for power-law exponents of $n=1$ and $n=3.5$.

For $L \gg h$, the wavelengths and growth rates approximate the case of a layer over a half-space, where $q'_{\max} = 0.097$ and $k'_{\max} = 1.69$ for $n=1$, using (32) to non-dimensionalize by h. This is to be expected, because, for large L, viscosity remains approximately constant with depth, and the system behaves as a layer over a half-space. Conversely, if $L \ll h$, the viscosity is strongly depth-dependent, and we must non-dimensionalize by L using (40). This gives $q'_{\max} = 0.13$ and $k'_{\max} = 0.89$, the solutions produced by (42) for the case of exponential decrease of viscosity with depth. For $L \ll h$, the system behaves as if there were no upper boundary. Between these extremes, dependence on both L and h is apparent.

6.2 Linear decay of density and exponential decay of viscosity

The inclusion of a linear density profile provides a more realistic representation of the lithosphere. Using the numerical approach, we can include linear density gradients by discretizing the density profile throughout many layers. Results using 50 layers are shown in Fig. 9, again for $n=1$ and $n=3.5$. For $L \gg h$, viscosity remains nearly constant throughout the medium, and $q'_{\max} = 0.037$ at $k'_{\max} = 2.2$ for $n=1$, as from (48).

A comparison of Figs 8(a) and 9(a) shows that the linear density profile does not significantly affect the wavelength of maximum growth rate. Growth rates for linearly decreasing density, however, are consistently the smaller (Figs 8b and 9b). This is probably due to the redistribution of mass throughout the layer. Instead of the instability growing from a perturbation at a single interface, it grows throughout the layer. For the case in which $h \gg L$, growth rates decrease with decreasing L; the increased viscosity of the upper part of the layer retards growth. Because we normalized the growth rate by the viscosity at the bottom of the layer, if L is small, only the bottom part of the layer can deform easily, and because of the small density difference across this region, the total potential energy available to drive the instability is small.

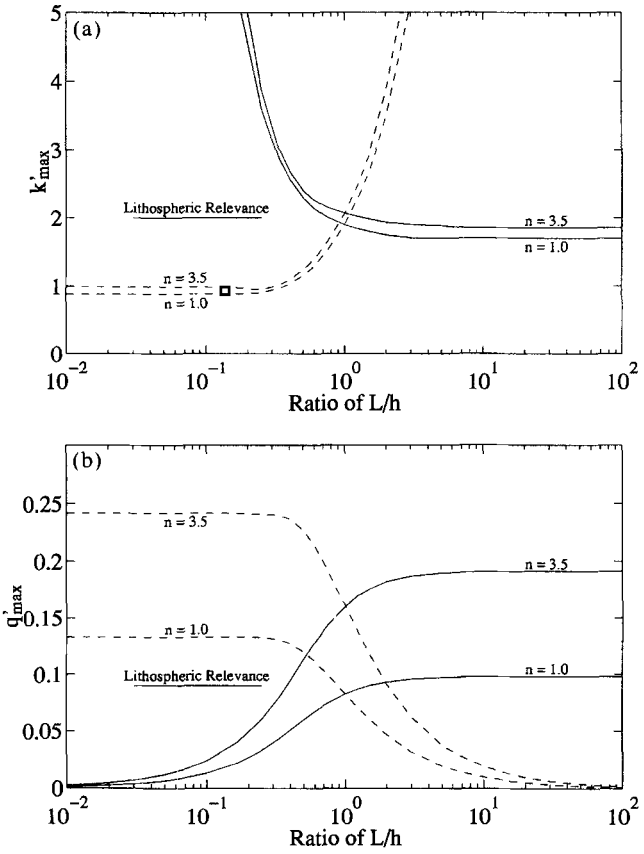

Figure 8. (a) Plot of k'_{max} versus the ratio L/h with $n=1$ and $n=3.5$ for a layer over a half-space with exponentially varying viscosity. The solid curves are non-dimensionalized by (32), using the layer height h. The dashed lines are non-dimensionalized by (40) using the viscosity decay length, L. End-member solutions on both sides reproduce the results shown in Figs 1 and 3 (see text). (b) Plot of q'_{max} versus the ratio L/h for the same viscosity structure. The range of L/h that is reasonable for the lithosphere is shown.

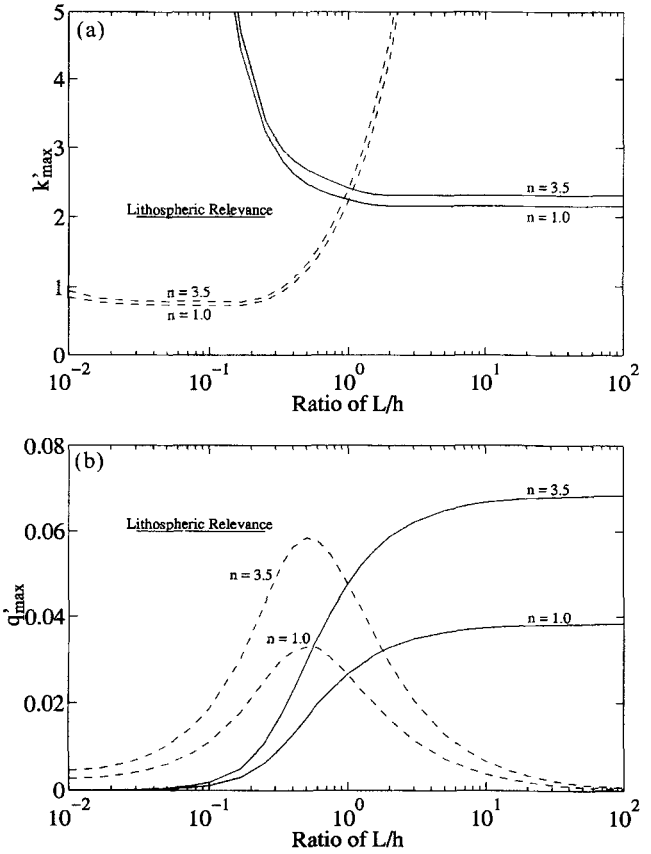

Figure 9. Similar to Fig. 8, for a linear decrease of density in the upper layer.

From another perspective, the viscosity of material affected by the perturbation increases as L decreases.

6.3 Free surface

We now consider a layer over a half-space with stress-free boundary conditions at the upper interface. These are now stress boundary conditions (25) and (27), in which we must specify the density discontinuity, $\Delta\rho_t$, across the upper interface. We express $\Delta\rho_t$ as a multiple of the density contrast across the bottom interface, $\Delta\rho_b$:

$$\theta = -\frac{\Delta\rho_t}{\Delta\rho_b}. \tag{56}$$

By definition, θ is positive. In addition, if $\theta < 1$, the net density contrast across the layered structure is negative, and, because the free surface allows sliding of the entire upper boundary, infinite growth rates at long wavelengths result. Thus, we only consider $\theta > 1$.

Growth rates are larger than we found for a rigid top because a free surface provides less resistance to deformation than does a rigid top; wavelengths for the free surface are also longer (Fig. 10). A comparison of analogous curves in Fig. 10 shows that larger viscosity contrasts, r, across the bottom interface produce faster growth rates; therefore the growth rate increases monotonically with decreasing viscosity of the material below the layer. Moreover, wavelengths of maximum growth rate lengthen with increasing r. As a result, the approximation of $r \to \infty$ by $r > 10$ is not valid for a layer with a free surface, as we found for a rigid top. In addition, plastic medium (large n) generally produces slightly shorter wavelengths but significantly faster dimensionless growth rates. Finally, dimensionless growth rates and wavelengths are relatively independent of the relative density contrasts given by θ, for $\theta > 5$.

Although the surface of the earth is, of course, a free surface, these results have only indirect application to the earth, because the strong upper lithosphere acts as a rigid top to the deforming lower lithosphere. These calculations, however, are useful because they can be compared to those for instabilities generated by horizontal strain rates, which require stress-free boundary conditions on the upper surface. This comparison follows.

7 THERMAL DIFFUSION

We have calculated characteristic wavelengths and growth rates for gravitational instabilities that grow from small fluctuations in density along horizontal interfaces. Because these density fluctuations are created by corresponding variations in temperature, thermal diffusion will tend to smooth out density anomalies from which instabilities can grow. Thus, gravitational instabilities will only grow if they can

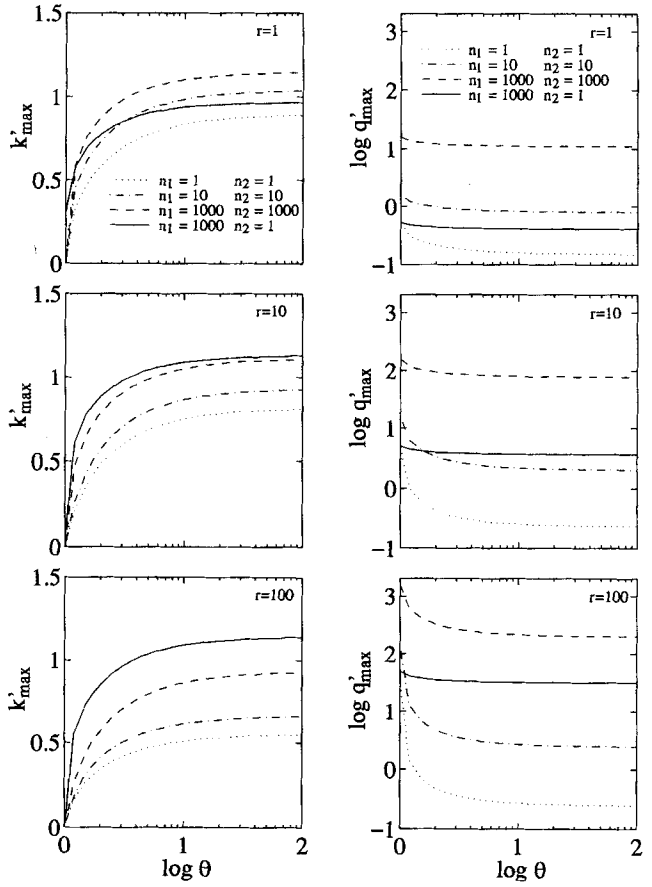

Figure 10. Plot of k'_{max} versus θ (left column) and q'_{max} versus θ (right column) for a layer over a half-space with a free surface. θ, defined by (56), is the ratio of density contrasts at the top and the bottom of the layer. Non-dimensionalization is by (32). Top, middle, and bottom rows show values for $r=1$, $r=10$, and $r=100$, respectively, where $r=\mu_1/\mu_2$ and the effective viscosities of the layer and the half-space are constant. Various combinations of the two power-law exponents n_1 and n_2 are shown.

do so faster than heat diffuses. The rate of heat diffusion can be estimated by a simple analysis of the heat diffusion equation.

We begin by defining a temperature fluctuation, $\tilde{T}$, as a perturbation to the background temperature field with sinusoidal dependence on x. We expect the temperature fluctuations to be a maximum at the interface on which they grow, and to decrease to zero at the surface of a layer, which is presumably at a fixed temperature. For simplicity, we will assume that $\tilde{T}$ exhibits a quarter-wavelength sinusoidal dependence on z:

$$\tilde{T}(x,z,t=0)=\tilde{T}_0\cos(kx)\cos\left(\frac{\pi z}{2h}\right), \tag{57}$$

where $\tilde{T}_0$ is an amplitude, k is a wavenumber and $z=h$ is the top of the layer. The time-dependent solution to the heat diffusion equation (Turcotte & Schubert 1982, p. 154),

$$\frac{\partial\tilde{T}(x,z,t)}{\partial t}=\kappa\left(\frac{\partial^2}{\partial x^2}+\frac{\partial^2}{\partial z^2}\right)\tilde{T}(x,z,t), \tag{58}$$

is simply

$$\tilde{T}(x,z,t)=\tilde{T}_0\exp(-q_t t)\cos(kx)\cos\left(\frac{\pi z}{2h}\right), \tag{59}$$

where q_t the rate at which thermal anomalies decay and is given by

$$q_t=\kappa\left(k^2+\frac{\pi^2}{4h^2}\right). \tag{60}$$

The first term of (60) represents horizontal thermal diffusion; the second term represents diffusion in the vertical direction.

To compare the decay rates of thermal diffusion with the growth rates of gravitational instabilities, we must non-dimensionalize q_t in the same manner we did q. Using (32) to non-dimensionalize by h, we find

$$q'_t=\frac{\mu\kappa}{\Delta\rho g h^3}\left(k'^2+\frac{\pi^2}{4}\right)=\frac{1}{R_h}\left(k'^2+\frac{\pi^2}{4}\right). \tag{61}$$

Here q'_t is the dimensionless decay rate of thermal diffusion. Because the amplitude of the growth rate resembles the inverse of a Rayleigh number, we define it as $1/R_h$. Non-dimensionalizing by L using (40), we find

$$q'_t=\frac{\mu\kappa}{\Delta\rho g L^3}\left(k'^2+\frac{\pi^2L^2}{4h^2}\right)=\frac{1}{R_L}\left(k'^2+\frac{\pi^2L^2}{4h^2}\right), \tag{62}$$

where the dimensionless number R_L also resembles a Rayleigh number.

Estimates of q'_t from (61) and (62) can be directly compared to previous calculations of q' because both represent dimensionless exponential growth rates (Fig. 11). Values of R_h or R_L less than about 1 produce thermal diffusion rates that are fast compared to growth rates of density instabilities. Thus, for $q'\leq q'_t$, thermal diffusion will tend to smooth out temperature anomalies faster than they can be advected, preventing the growth of density instabilities. If R_h or R_L are a few orders of magnitude larger than 1, we find $q'\geq q'_t$. In this case, density instabilities grow, but are slowed by thermal diffusion. We estimate the degree to which thermal diffusion affects growth rates by defining a net growth rate Q':

$$Q'=q'-q'_t. \tag{63}$$

Because of the quadratic dependence of q'_t on k', heat diffusion will suppress perturbations with large values of k' (short wavelengths), as shown in Fig. 11. As a result, the wavelength of maximum growth rate shifts towards longer wavelengths. For the longest wavelengths, thermal diffusion occurs more rapidly across the vertical extent of the layer than across horizontal perturbations. This vertical diffusion results in a non-zero intercept of q'_t with $k'=0$ (Fig. 11a). Vertical diffusion through the layer can suppress the growth of long-wavelength instabilities.

We examine the role of thermal diffusion in slowing maximum growth rates and lengthening their corresponding wavelengths by calculating Q'_{max} and k'_{max} as functions of R_h and R_L, for a suite of density and viscosity profiles analogous to those presented in Figs 8 and 9. For R_h or R_L greater than about 10^3, Q'_{max} and k'_{max} (Figs 12 and 13) approximately equal q'_{max} and k'_{max} as calculated assuming no thermal diffusion (Figs 8 and 9). Below this transitional value of R_h and R_L, growth rates and wavenumbers decrease. If h is the appropriate non-dimensionalization, total growth rates become negative

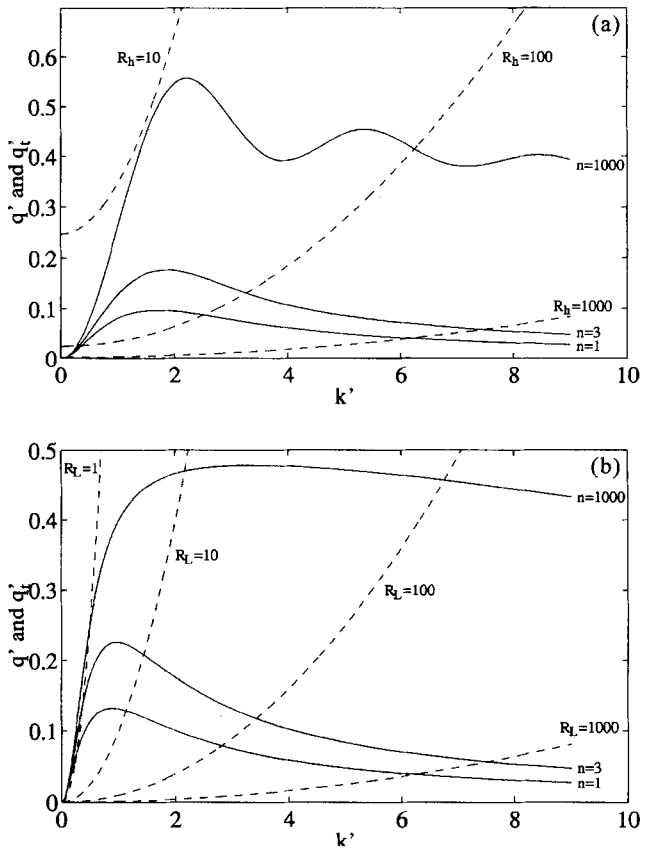

Figure 11. Plot of q' (solid lines) and q'_t (dashed lines) versus k' (a) for a layer of constant viscosity over a half-space and (b) for two half-spaces of different densities and continuous exponential decrease of viscosity with depth. For q', several values of n are shown, and the results are the same as those in Figs 2(a) and 5. For comparison, decay rates of perturbations due to thermal diffusion, q'_t, are shown, and are non-dimensionalized by (61) and (62). It is assumed in (b) that $L \ll h$, so the vertical diffusion of heat is ignored in this case. Several orders of magnitude of R_h and R_L are shown. Where $q' > q'_t$, we expect growth of temperature-induced density instabilities.

below values of R_h between 10 and 100 (Fig. 12), and Rayleigh–Taylor growth is effectively stopped. Wavelengths of maximum growth rate are increased by a factor of about 2 in this range. If L is the important length-scale, differences exist between constant and linear density profiles. Values of R_L as low as about 1 permit growth for the constant-density case (Fig. 13). For linear density profiles, thermal diffusion stops Rayleigh–Taylor growth at values of R_L between 10 and 100. For both profiles, if $L \ll h$, wavelengths of maximum growth rate can be several times those found without the inclusion of thermal diffusion, as values of k'_{max} close to zero are permitted.

8 THE ROLE OF HORIZONTAL STRAIN RATES

Horizontal compression or extension of a layered structure can cause unstable growth of folding or boudinage type deformation (Bassi & Bonnin 1988; Fletcher & Hallet 1983; Martinod & Davy 1992, 1994; Ricard & Froidevaux 1986; Smith 1975, 1977). Horizontal straining of a plastic layer produces growth rates that scale with the horizontal strain rate and wavelengths 4 to 6 times the thickness of the deforming layer (e.g. Martinod & Davy 1992; Ricard & Froidevaux 1986). We have already studied the case in which $\bar{\epsilon}_{xx}$ is zero or very small; we now increase $\bar{\epsilon}_{xx}$ to determine the magnitude of $\bar{\epsilon}_{xx}$ at which horizontal strain rates begin to dominate unstable growth. For these calculations, we use the numerical method described above. For simplicity, we include thermal diffusion in a qualitative discussion to follow.

The right-hand sides of boundary conditions (25) and (27) give the forcing terms for instabilities that result from horizontal strain rates and gravity, respectively. The vector **R** in (50) contains these forcing terms, which are incorporated into growth rates in the formation of matrix **P** in (54), and finally in the solution to (55). For simple layered structures, if the magnitude of the forcing term of one of (25) or (27) is much larger than the other, then it will dominate the elements of **P**. As a result, the style of deformation determined by the solution to (55) will also be controlled by this term.

The importance of the relative magnitudes of the gravitational and strain-rate forcing terms prompts us to define their ratio as a dimensionless number, f. In determining the ratio of the right-hand sides of (25) and (27), we note that the amplitude of the perturbation, η, cancels, and its derivative leaves a wavenumber, k. For folding, we expect the wavenumber to scale inversely with the layer thickness, h, so we use

$$f = \frac{\Delta\mu\bar{\epsilon}_{xx}}{\Delta\rho g h}. \tag{64}$$

If there are several interfaces on which instabilities can develop, the interface with the largest density discontinuity will dominate the growth of gravitational instabilities, if this density change is of favourable sign. Similarly, $\Delta\mu$ and h must correspond to the plastic layer that folds or thickens under compression or extension.

To illustrate the transition of behaviour for increasing values of f, we included $\bar{\epsilon}_{xx}$ in the analysis of a plastic layer ($n = 1000$) over a half-space with Newtonian viscosity. To allow folding or boudinage of this layer, we applied stress-free boundary conditions to the top surface, using (25) and (27) at z. To represent deformation of the mantle lithosphere, we used densities above, in, and below the layer of 2800, 3300, and 3250 kg m^{-3}, corresponding to densities of the crust, mantle lithosphere, and asthenosphere and giving $\theta = 14$ using (56). This value is well beyond the transitional value of about $\theta = 5$ above which maximum wavelengths are independent of θ. As we have shown, the ratio of viscosities between the layer and half-space does affect growth rates and wavelengths; we used $r = 100$.

Maximum growth rates and their corresponding wavelengths vary with f (Fig. 14), for both compression and extension. For $f \ll 1$, gravitational forcing dominates, and $q'_{max} = 32$ and $k'_{max} = 1.09$, or $\lambda_{max} = 5.7h$, consistent with the values of q'_{max} and k'_{max} found for the purely gravitational instability shown by the solid curve in Fig. 10 for $r = 100$. For large values of $\bar{\epsilon}_{xx}$ corresponding to $f \gg 1$, growth rates increase linearly with f. The characteristic wavenumber of $k'_{max} = 1.48$, corresponding to $\lambda_{max} = 4.2h$, for both compressional and extensional deformation, agrees with the results of Smith (1977) and Martinod & Davy (1994). The eigenvectors, **V**, associated with growth at this wavelength show that compression and extension produce folding and boudinage, respectively.

Between the two extremes presented above, the gravitational- and strain-rate-dependent instabilities compete, and the

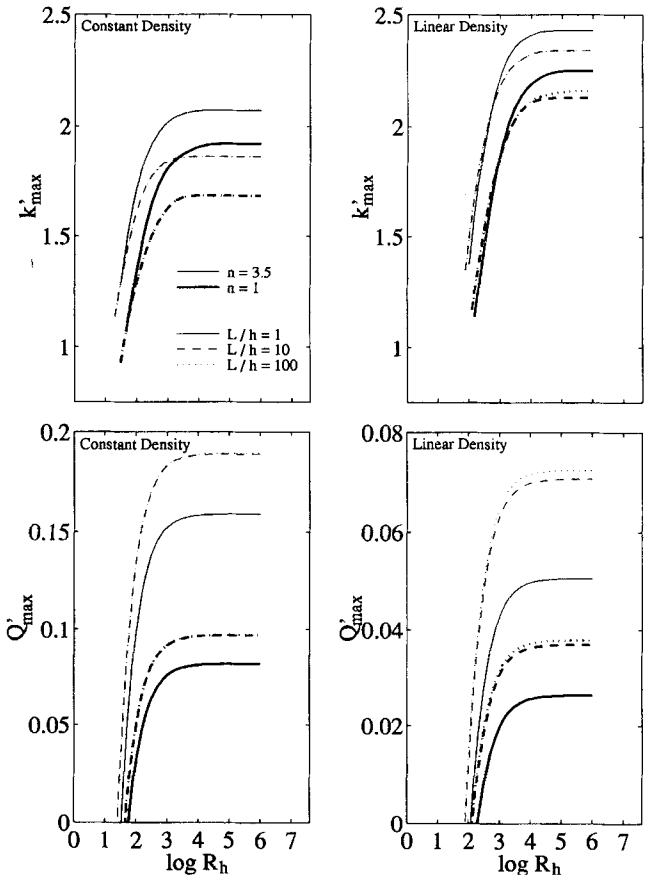

Figure 12. Plots showing how k'_{max} and Q'_{max} vary with R_h. Results are given for exponential decrease of viscosity in a layer and $L/h \geq 1$, as given by (63) and non-dimensionalized by (61) and (32). The left column shows results for a single density step at the bottom of the layer, while the right column shows those for a linear decrease in density across the layer. Thick lines indicate results for $n = 1$ and thin lines for $n = 3.5$. The ratio of L/h for each line is indicated. k'_{max} is not shown at values of R_h for which $Q'_{max} < 0$.

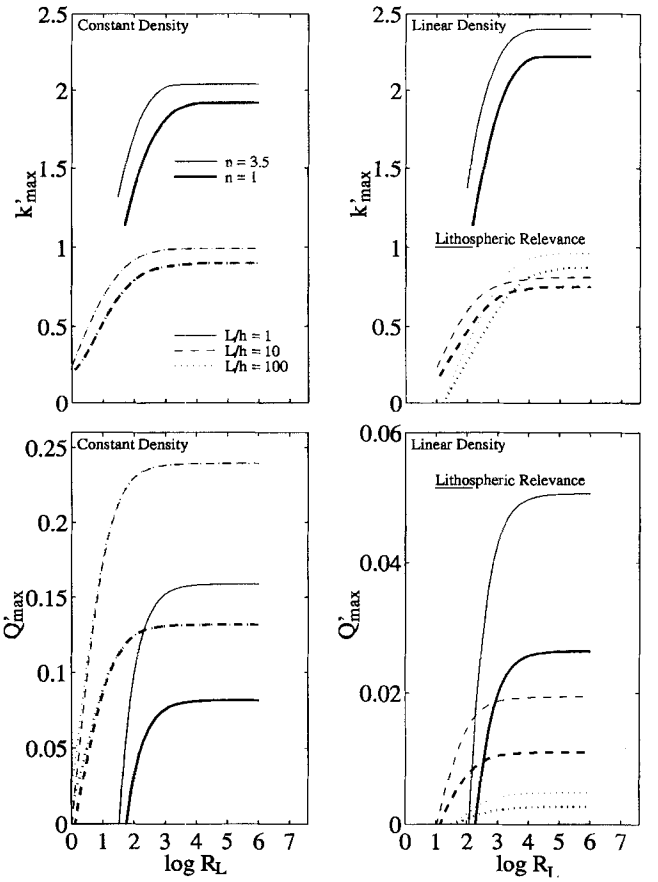

Figure 13. Similar to Fig. 12 for $L/h \leq 1$, using (62) and (40) for non-dimensionalization. A range of R_L appropriate for the lower lithosphere is indicated, as described in the text.

resulting deformation will be the result of some combination of the two. As shown in Fig. 14(a), this interplay between horizontal strain rates and gravitational instabilities shortens the characteristic wavelength for compression and slightly lengthens it for extension. This behaviour can be explained by the relative stability of folding and boudinage modes of deformation when strain-rate forcing becomes important. As shown by the eigenvector for small f, the top surface does not exhibit significant deformation under pure gravitational forcing. Such behaviour resembles boudinage in the lower half of an extending layer (Ricard & Froidevaux 1986). Folding of a layer in compression, however, deforms the upper surface significantly. As a result, when compression first begins to dominate growth, it must do so in the presence of a boudinage mode of deformation. This mode, however, does not grow rapidly for compression because compression tends to thicken the thin, and therefore weaker, regions of the layer, the 'pinches' in a 'pinch and swell' instability. In addition, boudinage grows most rapidly for compression at wavelengths shorter than those for folding (e.g. Martinod & Davy 1992; Ricard & Froidevaux 1986). In the range of f where compression begins to suppress Rayleigh–Taylor growth, both grow with comparable wavenumber but with opposite eigenvalues. As a result, maximum growth rates develop with quite different wavelengths. In particular, compression induces deformation similar to boudinage at wavelengths shorter than those generated by folding or gravitational instabilities. It is clear from Fig. 11 that the range of f over which this wavelength shift occurs can be several orders of magnitude.

The transition from gravitationally to strain-rate-induced instabilities with increasing $\bar{\epsilon}_{xx}$ is also apparent for structures resembling the lithosphere (Fig. 15). The model used here (Fig. 15) contains two layers overlying a half-space: a top layer of thickness h_1, plastic viscosity, a free surface, and constant viscosity, over a layer of thickness h_2 with Newtonian viscosity and exponential viscosity with decay length L. Density decreases linearly and continuously across both layers. A lower half-space with constant effective viscosity and density represents the asthenosphere. Non-dimensionalization is given by (40) because L is the relevant parameter in the gravitational instability. The relative values of h_1, h_2, and L will clearly affect the growth rates and wavelengths that form. To illustrate a transition between the two styles of deformation, we used $h_1 = h_2 = 12L$ and chose f such that both gravitational and strain-rate forcing are apparent.

Gravitational forcing of the type described above is evident in Fig. 15 at $q'_{max} = 0.009$ and $k'_{max} = 0.78$, or $\lambda_{max} = 8.1L$, and is consistent with our calculations for a layer with exponential viscosity and linear density dependence on depth (Fig. 9).

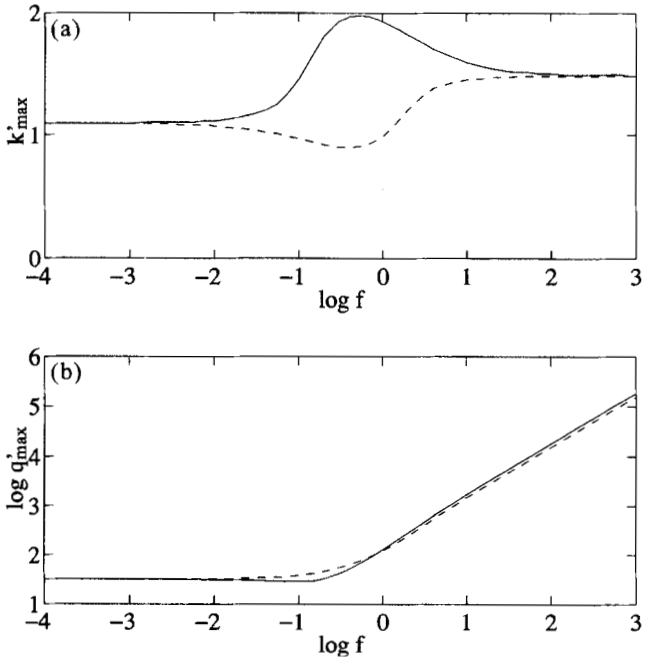

Figure 14. (a) Plot of k'_{max} versus f for a plastic layer ($n=1000$) with a free surface over a half-space with Newtonian viscosity, as described in the text. Non-dimensionalization is by (32). Solid lines represent compression and dashed lines represent extension. (b) Plot of q'_{max} versus f for the same layer. The relative amplitudes of deformation of the top and bottom interface are given by the elements of the eigenvector, **V**, which correspond to the maximum growth rate. For $f \ll 1$ (Rayleigh–Taylor), $\mathbf{V}=(0.05, 0.99)$; most of the deformation occurs on the bottom interface. For $f \gg 1$ and $\bar{\epsilon}_{xx}$ compressive, $\mathbf{V}=(0.71, 0.71)$. Thus, the two interfaces deform in parallel, and a folding instability develops. For $f \gg 1$ and $\bar{\epsilon}_{xx}$ extensive, $\mathbf{V}=(0.71, -0.71)$; the two interfaces deform in opposite directions, creating a boudinage instability. Thermal diffusion has been ignored.

Although the top surface is free, the density instability occurs at the bottom of the lithosphere, and the high-viscosity upper layer serves as a rigid top. Thus, the growth rates and wavelengths which occur for small horizontal strain rates are closer to those for a rigid top than for the free surface. If horizontal strain rates are large enough, the plastic layer begins to undergo folding or boudinage at long wavelengths; in Fig. 15, $\lambda_{max}=63L=5.2h_1$ for compression and $\lambda_{max}=43L=3.5h_1$ for extension. These are consistent with Martinod & Davy's (1992) estimate of $\lambda_{max} \approx 4h$, with shorter wavelengths for boudinage than for folding.

The growth rates of the folding and boudinage modes scale with the horizontal strain rate and thus will grow proportionally with f. For values of f greater than those used in Fig. 15, the instabilities that grow fastest will be those induced by horizontal strain rates. The transition between gravitational and strain-rate instabilities occurs at some critical value of f. At this value, the growth rates of the folding or boudinage modes, which scale with f, become larger than the growth rate of the Rayleigh–Taylor mode, which does not change with f. In the example shown in Fig. 15, the transition between styles of deformation occurs for $f \approx 1$, with higher critical values of f for extension than for compression, because of slightly faster growth rates for folding, as Smith (1977) predicted.

The inclusion of thermal diffusion in the calculations for Figs 14 and 15 would, as we have seen, reduce the maximum growth

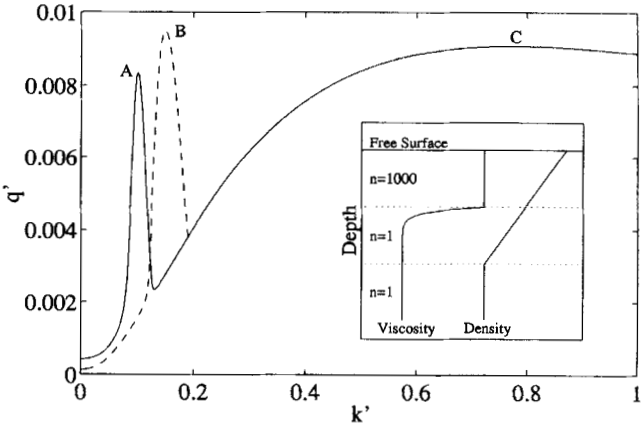

Figure 15. Plot of q'_{max} versus k' for the lithospheric model described in the text and shown in cartoon form in the inset. Non-dimensionalization is by (40), and thermal diffusion is ignored. Transitional values of the horizontal strain rate, $\bar{\epsilon}_{xx}$, are shown: the critical value of $\bar{\epsilon}_{xx}$ occurs for $f=0.7$ for compression (solid line) and $f=2.0$ for extension (dashed line). Three peaks are apparent: Peak A is induced by compression and represents folding, Peak B is induced by extension and represents boudinage, and Peak C is generated by the gravitational instability at the bottom of the lithosphere. Peaks A and B, because they are induced by horizontal strain rates, have growth rates which scale with $\bar{\epsilon}_{xx}$, while the growth rate of Peak C is independent of $\bar{\epsilon}_{xx}$. Thus, for values of f larger than those presented here, folding or boudinage overwhelms Rayleigh–Taylor growth.

rates and increase the wavelengths at which they occur for gravitationally induced instabilities. Depending on the relevant values of R_h, the reduction in growth rates can range from insignificant to complete. If growth rates are slowed, but not stopped, we can expect them to be reduced by a factor of about 2 or 3, as seen in Fig. 12. From Fig. 14, a factor of 2 or 3 slowing of the growth rate will result in a decrease in the transitional value of f by a similar factor. A decrease in f by an order of magnitude requires values of R_h close to the point at which Rayleigh–Taylor growth stops completely. Because we have not constrained the transitional value of f to an order of magnitude, we do not expect thermal diffusion to significantly change our estimation of the transitional value of f, unless it does so by completely halting Rayleigh–Taylor growth. In that case, strain-rate-induced instabilities dominate throughout the entire range of f.

9 APPLICATION TO THE LITHOSPHERE

As discussed above, the lithosphere is characterized by both an approximately exponential decrease of viscosity and a linear decrease in density with depth. The exponential decay constant, of the order of 5 to 12 km, is much smaller than the thickness of continental lithosphere, which could be of the order of 100–300 km, 10 to 30 per cent of which is continental crust. With a density gradient between -0.5 and -1.5 kg m^{-3} km^{-3} for the mantle lithosphere, an appropriate model for deformation in the lower half of the mantle lithosphere, ignoring thermal diffusion, is used in Fig. 9, with h between 50 and 150 km, L between 5 and 12 km, and $n=3.5$. Thus, the ratio L/h can reasonably vary between $5/150=0.03$ and $12/50=0.25$. From Fig. 9, we find that k'_{max}, which does not vary with the ratio L/h in this range, must be about 0.8, giving $\lambda_{max}=7.8L$, and corresponding to dominant wavelengths between 40 and 90 km.

This wavelength range provides a lower bound on the permitted wavelengths of maximum growth rate for the case in which thermal diffusion is negligible. This range requires values of R_L greater than about 10^4, as shown in Fig. 13 for linear density and $n=3.5$. Smaller values of R_L force longer wavelengths by damping out the shorter ones. To obtain a reasonable range in R_L, we assume a viscosity at the base of the lithosphere of $\mu_b = 10^{19}$ Pa s (e.g. Hager 1991) and $\Delta\rho = 75$ kg m^{-3} to the definition of R_L in (62). R_L can reasonably vary between about 9, using $L=5$ km, and 400, using $L=12$ km. Of the parameters included in the calculation of R_L, μ_b is the most poorly constrained and could vary from Hager's (1991) value by an order of magnitude, thus increasing the possible range R_L. Applying this range in R_L to Fig. 13 for linear density, $n=3.5$ and $L/h=0.1$, we expect wavenumbers to vary between $k'_{max}=0.25$ for $L\approx 5$ km and $k'_{max}=0.7$ for $L\approx 12$ km. Both extremes produce $\lambda_{max}\approx 100$ km. If the ratio L/h is less than 0.1, smaller values of k'_{max} are available, which produce longer wavelengths. To achieve low values of L/h, L must be small, so significantly longer wavelengths are not likely. Wavelengths of $\lambda_{max}=200$ km seems to be a maximum, achieved by a conspiracy of $L\approx 7$ km, $h\approx 150$ km, $R_L\approx 30$, giving $k'_{max}\approx 0.2$. Lowering viscosities below Hager's 10^{19} Pa s value should shift the range of wavelengths towards smaller values. Higher viscosity could force part of the range in R_L to fall below $R_L=10$, the approximate minimum value for which density instabilities can grow. In this case, only for large values of L will Rayleigh–Taylor growth occur. At the extreme, values of L near 12 km, combined with $k'_{max}=0.25$ could produce wavelengths up to 300 km. If asthenospheric viscosities are greater than 10^{21} Pa s, the growth of density instabilities will be stopped completely.

Unlike wavenumbers, growth rates Q'_{max} vary significantly with the ratio L/h, as well as with R_L (Figs 9 and 13). From Fig. 13, we estimate a maximum value of non-dimensionalized total growth rate of $Q'_{max}=0.02$. Minimum growth rates are, of course, zero for a range of lithospheric structures with $R_L < 10$. Using (40) and the parameter values above, we estimate a maximum growth rate of 4×10^{-14} s^{-1}. As before, μ_b is poorly constrained, so maximum growth rates for gravitational instabilities in the lithosphere could range from 10^{-14} s^{-1} to zero, which corresponds to e-folding timescales of three million years and higher. Because of exponential growth, this range of growth rates places the Rayleigh–Taylor instability as a descriptor of lithospheric downwellings on a scale of relevance between negligible importance and dominance.

Detection of Rayleigh–Taylor instabilities at the base of the lithosphere from measurements at the surface of the Earth is likely to be difficult. Turcotte & Schubert (1982, p. 123) estimate the length-scale for compensation of surface loads on a typical lithosphere with flexural rigidity $D=10^{23}$ N m to be about 420 km. Loads exceeding this wavelength and generated at the bottom of the lithosphere would be expected to be compensated at the surface. Lithospheric Rayleigh–Taylor instabilities, as described above, generate loads of shorter wavelength, and thus would not be expected to produce measurable surface deformation.

The gravity signal of perturbations at wavelengths expected for Rayleigh–Taylor growth is unlikely to be detected. Density perturbations at depth z and of wavelength λ produce a gravitational signal that decreases as $\exp(-2\pi z/\lambda)$ (Turcotte & Schubert 1982, p. 221). Consider a perturbation with a density anomaly of about 50 kg m^{-3}, at a depth of about 100 km, a range of wavelengths between 100 and 200 km, and an amplitude of the order of 20 km. The surface Bouguer gravity anomaly associated with this density anomaly is between 10^{-2} and 10^{0} mgal, with higher values for longer wavelengths. Terrain corrections in mountainous regions have uncertainties which are much larger than this.

We have shown that as horizontal strain rates increase, they begin to overwhelm the growth of Rayleigh–Taylor-type instabilities. The transition from gravitationally to strain-rate-induced instabilities occurs when the ratio of their forcing terms, expressed by the dimensionless factor f in (64), reaches some transitional value. Figs 14 and 15 show transitional values of f between 0.1 and 1, but we can assume that lithospheric structures exhibit a range of transitional values of f. In addition, we have seen that diffusion of heat can be expected to decrease transitional values of f by a factor of 2 or more. Using (64), with $\Delta\rho=50$ kg m^{-3}, $\mu=10^{22}$ Pa s for the viscosity of the mantle lithosphere, $h=50$ km to address folding of upper lithosphere, and with a critical value of f between 0.1 and 1, horizontal strain rates of 10^{-15} to 10^{-16} s^{-1} are necessary for these horizontal strain rates to control unstable growth. Because we have not adequately constrained f, and because of the uncertainty in asthenospheric viscosity, this figure is approximate. A compressional strain rate of $\bar{\epsilon}_{xx}=10^{-15}$ s^{-1} requires shortening by a factor of 2 in 30 million years, as seems to characterize Tibet (Molnar, England & Martinod 1993). For horizontal strain rates greater than the critical value, wavelengths significantly longer than those predicted by Rayleigh–Taylor analysis are possible, with growth rates that scale with the horizontal strain rate.

Lithospheric instabilities produced by horizontal strain rates typically exhibit wavelengths 4 to 6 times the effective thickness of the lithosphere (Martinod & Davy 1992). Thus, we expect folding and boudinage to occur with wavelengths of the order of 4 to 6 times 50 km, or 200 to 300 km, typical of widths of regional mountain belts. These instabilities are also more likely to produce significant surface deformation than are density instabilities because they directly deform the surface. This observation, however, does not diminish the possible importance of density instabilities in the growth of surface structures. At finite amplitudes, perturbations in density might grow at the bottom of the lithosphere, below the region of folding and boudinage at the surface. In this way, horizontal shortening could serve to promote the growth of long-wavelength density instabilities by creating an initial perturbation from which these density instabilities can grow.

10 CONCLUSIONS

Gravitational instabilities at the bottom of the lithosphere grow at rates that depend on viscosity, the rapidity with which this viscosity decreases with depth, and the magnitude of the density inversion which creates them. The wavelength of the fastest-growing deformation is about eight times the length-scale for the exponential decay of viscosity. Thermal diffusion suppresses the growth of such wavelengths and therefore lengthens those of maximum growth rate to a range between 100 and 200 km for continental lithosphere, with wavelengths of 300 km possible for particular sets of lithospheric parameters. Because these disturbances occur

at depths comparable to their horizontal length-scales, we would not expect them to produce a significant surface deformation. Deformation grows exponentially with e-folding times as low as three million years, depending on the viscosity assumed for the bottom of the lithosphere, and the e-folding length of viscosity. Such rapid growth rates could destroy lateral heterogeneity in the bottom part of the mantle lithosphere. Alternatively, the acceptable range of lithospheric parameters allows thermal diffusion to smooth over temperature-induced density perturbations, thus preventing the growth of Rayleigh–Taylor instabilities.

These growth rates and wavelengths are applicable only if Rayleigh–Taylor instabilities grow more rapidly than disturbances that grow due to horizontal stretching or shortening of the lithosphere. For significantly rapid horizontal compression or extension, instabilities with longer wavelengths develop and overwhelm the Rayleigh–Taylor growth. We estimate this transitional strain rate to be in the range of 10^{-15} to 10^{-16} s^{-1}, corresponding to shortening or extension of 100 per cent in 30 to 300 million years. These strain rates are comparable to strain rates observed in tectonically active regions of the Earth.

Mechanical thickening of the lithosphere could induce long-wavelength instabilities at the bottom of the lithosphere which, at large amplitudes, would pinch off and fall into the mantle, causing the overlying material to converge and create rapid surface uplift (England & Houseman 1989; Fleitout & Froidevaux 1982; Houseman *et al.* 1981). Such rapid uplift may have occurred 5 to 10 million years ago on the Tibetan Plateau, over a region hundreds of kilometres wide (Harrison *et al.* 1992; Molnar *et al.* 1993). Our results suggest that significantly shorter wavelengths would dominate a strictly Rayleigh–Taylor representation of this instability. The inclusion of thermal diffusion can serve to lengthen wavelengths of maximum growth rate, but wavelengths as large as the widths of major mountain belts seem difficult to achieve.

Our analysis is restricted to small amplitudes, and does not fully integrate gravitational instability and thermal diffusion as they must be in a complete convection calculation. If long-wavelength perturbations are to grow, they must do so under conditions for which a linear analysis of a Rayleigh–Taylor instability is inappropriate. Significant horizontal compression or extension can generate wavelengths comparable to the width of mountain ranges. In addition, convective heat transfer could impose flow at long wavelengths or generate long-wavelength perturbations that could grow as gravitational instabilities. If the spectrum of initial perturbations is shifted heavily towards long wavelengths by tectonic or convective processes, these long-wavelength perturbations could reach finite amplitudes before more rapidly growing perturbations at shorter wavelengths because they begin growth from larger amplitudes.

ACKNOWLEDGMENTS

We thank P. England, B. Hager, G. Houseman, G. Jarvis, J. Pedlosky, and J. Whitehead and one anonymous reviewer for thoughtful insights which have helped to improve this paper. In particular, a review by Jarvis pointed out the qualitative effect of thermal diffusion. This work was supported in part by NSF grant EAR 94-06026, NASA DOSE grant NAG5-1911, and by a National Science Foundation Graduate Research Fellowship.

REFERENCES

Bassi, G. & Bonnin, J., 1988. Rheological modeling and deformation instability of lithosphere under extension, *Geophysical Journal,* **93,** 485–504.

Biot, M.A., 1961. Theory of folding of stratified viscoelastic media and its implication in tectonics and orogenesis, *Geol. Soc. Am. Bull.,* **72,** 1595–1620.

Burchfiel, B.C., Cowan, D.S. & Davis, G.A., 1992. Tectonic overview of the Cordilleran orogen in the western United States, in *The Cordilleran Orogen: Conterminous U.S.,* pp. 407–479, eds Burchfiel, B.C., Lipman, P.W. & Zoback, M.L., The Geological Society of America, Boulder, CA.

Burov, E.V., Kogan, M.G., Lyon-Caen, H. & Molnar, P., 1990. Gravity anomalies, the deep structure, and dynamic processes beneath the Tien-Shan, *Earth planet. Sci. Lett.,* **96,** 367–383.

Chandrasekhar, S., 1961. *Hydrodynamic and Hydromagnetic Stability,* Oxford University Press, Oxford.

England, P. & Houseman, G., 1989. Extension during continental convergence, with application to the Tibetan Plateau, *J. geophys. Res.,* **94,** 17 561–17 579.

Fleitout, L. & Froidevaux, C., 1982. Tectonics and topography for a lithosphere containing density heterogeneities, *Tectonics,* **1 (1),** 21–56.

Fletcher, R.C., 1974. Wavelength selection in the folding of a single layer with power law rheology, *Am. J. Sci.,* **274,** 1029–1043.

Fletcher, R.C. & Hallet, B., 1983. Unstable extension of the lithosphere: A mechanical model for Basin-and-Range structure, *J. geophys. Res.,* **88,** 7457–7466.

Hager, B.H., 1991. Mantle viscosity: A comparison of models from postglacial rebound and from the geoid, plate driving forces, and advected heat flux, in *Glacial Isostasy, Sea-Level and Mantle Rheology,* pp. 493–513, eds Sabadini, R., Lambeck, K. & Boschi, E., Kluwer Academic Publishers, Dordrecht.

Harrison, T., Copeland, P., Kidd, S. & Yin, A., 1992. Raising Tibet, *Science,* **255,** 1663–1670.

Houseman, G.A., McKenzie, D.P. & Molnar, P., 1981. Convective instability of a thickened boundary layer and its relevance for the thermal evolution of continental convergent belts, *J. geophys. Res.,* **86,** 6115–6132.

Kohlstedt, D.L., Evans, B. & Mackwell, S.J., 1995. Strength of the lithosphere: Constraints imposed by laboratory experiments, *J. geophys. Res.,* **100,** 17 587–17 602.

Martinod, J. & Davy, P., 1992. Periodic instabilities during compression or extension of the lithosphere, 1. Deformation modes from an analytical perturbation method, *J. geophys. Res.,* **97,** 1999–2014.

Martinod, J. & Davy, P., 1994. Periodic instabilities during compression or extension of the lithosphere, 2. Analogue experiments, *J. geophys. Res.,* **99,** 12 057–12 069.

Molnar, P. & Tapponnier, P., 1975. Cenozoic tectonics of Asia: Effects of a continental collision, *Science,* **189,** 419–426.

Molnar, P., England, P. & Martinod, J., 1993. Mantle dynamics, uplift of the Tibetan Plateau, and the Indian monsoon, *Rev. Geophys.,* **31 (4),** 357–396.

Ricard, Y. & Froidevaux, C., 1986. Stretching instabilities and lithospheric boudinage, *J. geophys. Res.,* **91,** 8314–8324.

Smith, R.B., 1975. Formation of folds, boudinage, and mullions in non-Newtonian materials, *Geol. Soc. Am. Bull.,* **86,** 1601–1609.

Smith, R.B., 1977. Unified theory of the onset of folding, boudinage, and mullion structure, *Geol. Soc. Am. Bull.,* **88,** 312–320.

Stacey, F.D., 1992. *Physics of the Earth,* Brookfield Press, Brisbane.

Turcotte, D.L. & Schubert G., 1982. *Geodynamics,* John Wiley and Sons, New York, NY.

Whitehead, J.A. & Luther, D.S., 1975. Dynamics of laboratory diapir and plume models, *J. geophys. Res.,* **80,** 705–717.

Zuber, M., 1987. Compression of oceanic lithosphere: An analysis of intraplate deformation in the central Indian basin, *J. geophys. Res.,* **92,** 4817–4825.

Zuber, M., Parmentier, E.M. & Fletcher, R.C., 1986. Extension of continental lithosphere: A model for two scales of Basin and Range deformation, *J. geophys. Res.*, **91**, 4826–4838.

APPENDIX A: FIRST-ORDER EXPRESSIONS OF STRESS AND STRAIN RATE

The zero-order terms of an expansion of the flow produced by horizontal compression, $\bar{\epsilon}_{xx}$, produce a basic state of pure shear (Smith 1977). Consider the first-order terms of the expansion, which provide information on the behaviour of perturbations to this state (Fletcher 1974). Then (4) becomes

$$\sigma_{xx}=\bar{\sigma}_{xx}+\tilde{\sigma}_{xx}=2\left(\bar{\mu}+\frac{\partial\bar{\mu}}{\partial\bar{\epsilon}_{xx}}\tilde{\epsilon}_{xx}\right)(\bar{\epsilon}_{xx}+\tilde{\epsilon}_{xx})-(\bar{p}+\tilde{p}),$$

$$\sigma_{zz}=\bar{\sigma}_{zz}+\tilde{\sigma}_{zz}=2\left(\bar{\mu}+\frac{\partial\bar{\mu}}{\partial\bar{\epsilon}_{xx}}\tilde{\epsilon}_{zz}\right)(\bar{\epsilon}_{zz}+\tilde{\epsilon}_{zz})-(\bar{p}+\tilde{p}), \tag{A1}$$

$$\sigma_{xz}=\bar{\sigma}_{xz}+\tilde{\sigma}_{xz}=2\left(\bar{\mu}+\frac{\partial\bar{\mu}}{\partial\bar{\epsilon}_{xx}}\tilde{\epsilon}_{xz}\right)(\bar{\epsilon}_{xz}+\tilde{\epsilon}_{xz}).$$

From (8),

$$\frac{\partial\bar{\mu}}{\partial\bar{\epsilon}_{xx}}=\frac{1}{2}A^{-1/n}\left(\frac{1-n}{n}\right)(\bar{\epsilon}_{xx})^{(1-2n)/n}\exp\left(\frac{E_a\beta z}{nRT_0^2}\right)=\frac{1-n}{n}\frac{\bar{\mu}}{\bar{\epsilon}_{xx}}. \tag{A2}$$

Applying (A2) to (A1) gives

$$\bar{\sigma}_{xx}+\tilde{\sigma}_{xx}=2\bar{\mu}\left[\bar{\epsilon}_{xx}+\tilde{\epsilon}_{xx}+\frac{1-n}{n}\left(\tilde{\epsilon}_{xx}+\frac{\tilde{\epsilon}_{xx}^2}{\bar{\epsilon}_{xx}}\right)\right]-(\bar{p}+\tilde{p}),$$

$$\bar{\sigma}_{zz}+\tilde{\sigma}_{zz}=2\bar{\mu}\left[\bar{\epsilon}_{zz}+\tilde{\epsilon}_{zz}+\frac{1-n}{n}\left(\frac{\tilde{\epsilon}_{xx}\bar{\epsilon}_{zz}}{\bar{\epsilon}_{xx}}+\frac{\tilde{\epsilon}_{xx}\tilde{\epsilon}_{zz}}{\bar{\epsilon}_{xx}}\right)\right]-(\bar{p}+\tilde{p}),$$

$$\bar{\sigma}_{xz}+\tilde{\sigma}_{xz}=2\bar{\mu}\left[\bar{\epsilon}_{xz}+\tilde{\epsilon}_{xz}+\frac{1-n}{n}\left(\frac{\tilde{\epsilon}_{xx}\bar{\epsilon}_{xz}}{\bar{\epsilon}_{xx}}+\frac{\tilde{\epsilon}_{xx}\tilde{\epsilon}_{xz}}{\bar{\epsilon}_{xx}}\right)\right]. \tag{A3}$$

We can simplify (A3) by subtracting the basic state:

$$\bar{\sigma}_{xx}=2\bar{\mu}\bar{\epsilon}_{xx}-\bar{p},\qquad \bar{\sigma}_{zz}=2\bar{\mu}\bar{\epsilon}_{zz}-\bar{p},\qquad \bar{\sigma}_{xz}=2\bar{\mu}\bar{\epsilon}_{xz}=0. \tag{A4}$$

Eliminating second-order terms, and using incompressibility yields (13), from which we calculate the growth of perturbations to the basic flow.

APPENDIX B: STRESS BOUNDARY CONDITIONS

Stress must be continuous across a boundary. If the z-component of that boundary is perturbed by deformation given by

$$\eta=\eta_0\cos(kx), \tag{B1}$$

then the stress must be continuous across this perturbed boundary. Because the boundary slopes, the total shear stress on one side of the boundary is given, to first order, by

$$\sigma_{xz}=\bar{\sigma}_{xz}+\frac{\partial\eta}{\partial x}(\bar{\sigma}_{xx}-\bar{\sigma}_{zz}). \tag{B2}$$

Continuity of shear stress, using (B2) and (7), yields

$$\tilde{\sigma}_{1,xz}-\tilde{\sigma}_{2,xz}=4\bar{\epsilon}_{xx}\frac{\partial\eta}{\partial x}(\bar{\mu}_1-\bar{\mu}_2). \tag{B3}$$

Similarly, continuity of normal stress across the perturbed boundary yields

$$\tilde{\sigma}_{1,zz}-\tilde{\sigma}_{2,zz}=-(\rho_1-\rho_2)g\eta. \tag{B4}$$

These boundary conditions contain information about the forces that amplify perturbations to the basic flow. If there is a horizontal strain rate, $\bar{\epsilon}_{xx}$, then the shear stresses (B3) create instabilities of a folding or boudinage type (e.g. Ricard & Froidevaux 1986). If there is a density discontinuity, $(\rho_1-\rho_2)$, perturbations are amplified by normal stresses (B4). If both forces are present, which of them dominates depends on their relative magnitudes.

APPENDIX C: SOLUTION METHOD

For flow within a layer, Bassi & Bonnin (1988) suggest a solution to (22):

$$W=A\cos(\beta kz)\,e^{\alpha' kz}+B\frac{\sin(\beta kz)}{\beta k}e^{\alpha' kz}+C\cos(\beta kz)\,e^{\alpha'' kz}+D\frac{\sin(\beta kz)}{\beta k}e^{\alpha'' kz}, \tag{C1}$$

where W gives the z dependence of $\tilde{w}$, and

$$\beta=\frac{r}{a},\qquad \alpha'=a-\frac{m}{2},\qquad \alpha''=-a-\frac{m}{2},$$

$$r=\left(\frac{m^2}{4}+\frac{n-1}{n^2}\right)^{1/2}, \tag{C2}$$

$$a=\left\{\frac{m^2}{8}+\frac{1}{n}-\frac{1}{2}+\frac{1}{2}\left[\frac{m^4}{16}+\frac{m^2}{2}\left(\frac{2}{n}+1\right)+1\right]^{1/2}\right\}^{1/2},$$

$$m=\frac{\gamma}{k}=\frac{1}{kL}. \tag{C3}$$

From this solution for W, we calculate $\tilde{w}$, $\tilde{u}$, $\tilde{\sigma}_{xz}$, and $\tilde{\sigma}_{zz}$ from (17), (26), and (28). These solutions are applied to the boundary conditions (23) to (25) and (29).

For a layer over a half-space, with a rigid boundary at the top, $z=h$, we use (C1) to solve for the flow in both layers, letting E, F, G, and H replace A, B, C, and D, in the solution to flow in the lower layer. To prevent divergence of W at large negative z, $G=H=0$. We use (32) to non-dimensionalize the analysis. Among the boundary conditions (23) to (25) and (29), $\tilde{w}_1(h)=0$ gives

$$A\cos(\beta_1 k')\,e^{\alpha_1 jk'}+B\frac{\sin(\beta_1 k')}{\beta_1 k}e^{\alpha_1 jk'}+C\cos(\beta_1 k')\,e^{\alpha_1' ik'}+D\frac{\sin(\beta_1 k')}{\beta_1 k}e^{\alpha_1' ik'}=0. \tag{C4}$$

$\tilde{u}_1(h)=0$ gives

$$\left[\left(A\alpha_1'+B\frac{1}{k}\right)\cos(\beta_1 k')-\left(B\frac{\alpha_1'}{\beta_1 k}-A\beta_1\right)\sin(\beta_1 k')\right]e^{\alpha_1 ik_i}+\left[\left(C\alpha_1''+D\frac{1}{k}\right)\cos(\beta_1 k')-\left(D\frac{\alpha_1''}{\beta_1 k}-C\beta_1\right)\sin(\beta_1 k')\right]e^{\alpha_1' ik_i}=0. \tag{C5}$$

Table 1. Symbols.

x, z	Space coordinates
$\mathbf{u} = (u, w)$	Velocity, with the x and z-components
$\rho, \Delta\rho = (\rho_1 - \rho_2)$	Density, density difference
$\mu, \Delta\mu = (\mu_1 - \mu_2)$	Viscosity, viscosity difference
n	Power law exponent for stress-strain rheology
h	Thickness a layer
$L = 1/\gamma$	Viscosity decay length
q	Growth rate for Rayleigh-Taylor instabilities
$q' = q\frac{\mu_1}{\Delta\rho g h}$ and $q' = q\frac{\mu_1\gamma}{\Delta\rho g}$	Dimensionless growth rate using length scales h and L
$q'_{\max}$	Maximum growth rate
$q'_t = \kappa\left(k^2 + \frac{\pi^2}{4h^2}\right)$	Exponential decay rate of temperature anomalies by thermal diffusion
$Q' = q' - q'_t$	Total growth rate, nondimensionalized in the same manner as q'
$R_h = \frac{\Delta\rho g h^3}{\mu\kappa}$ and $R_L = \frac{\Delta\rho g L^3}{\mu\kappa}$	Dimensionless number describing the relative roles of thermal diffusion and advection, using length scales h and L
k	Wave number of Fourier component
$k' = kh$ or $k' = kL$	Dimensionless wave number for the two length scales
$k'_{\max} = 2\pi/\lambda_{\max}$	Wavenumber, wavelength of maximum growth rate
$\tilde{p}, \tilde{\sigma}_{ij}, \tilde{\dot{\epsilon}}_{ij}$	Perturbation to hydrostatic pressure, stress tensor, strain rate tensor
$\bar{\dot{\epsilon}}_{xx}$	Horizontal strain rate due to tectonic forces
$q_j, \mathbf{V}_j$	Eigenvalues and eigenvectors corresponding to growth rates and amplitudes of perturbations of interfaces
$f = \frac{\Delta\mu\bar{\dot{\epsilon}}_{xx}}{\Delta\rho g h}$	Ratio relating strain rate forcing to gravitation forcing
$\theta = -\frac{\Delta\rho_t}{\Delta\rho_b}$	Ratio of density contrasts above and below a layer.
$r = \mu_1/\mu_2$	Ratio of the viscosity in a layer to that of the material below it.

$\tilde{w}_1(0) = \tilde{w}_2(0)$ gives

$$A + C - E = 0. \tag{C6}$$

$\tilde{u}_1(0) = \tilde{u}_2(0)$ gives

$$A\alpha'_1 + B/k + C\alpha''_1 + D/k - E\alpha'_2 - F/k = 0. \tag{C7}$$

$\tilde{\sigma}_{1,xz}(0) = \tilde{\sigma}_{2,xz}(0)$ gives

$$\bar{\mu}_1(0)\left[A(1+\alpha_1'^2-\beta_1^2) + B\frac{2\alpha'_1}{k} + C(1+\alpha_1''^2-\beta_1^2) + D\frac{2\alpha''_1}{k}\right]$$
$$-\bar{\mu}_2(0)\left[E(1+\alpha_2'^2-\beta_2^2) + F\frac{2\alpha''_2}{k}\right] = 0. \tag{C8}$$

$\tilde{\sigma}_{1,zz}(0) - \tilde{\sigma}_{2,zz}(0) + \tilde{w}_2(0)\bar{\mu}_1(0)/(q'h) = 0$ gives

$$\bar{\mu}_1(0)\left(AkM_1^{(1)} + B\frac{M_1^{(2)}}{\beta_1} + CkM_1^{(3)} + D\frac{M_1^{(4)}}{\beta_1} + \frac{E}{q'h}\right)$$
$$-\bar{\mu}_2(0)\left(EkM_2^{(1)} + F\frac{M_2^{(2)}}{\beta_1}\right) = 0, \tag{C9}$$

where

$$M^{(1)} = \left(\frac{4}{n} - 1\right)\alpha' - m(1 + \alpha'^2 - \beta^2) - \alpha'(\alpha'^2 - 3\beta^2),$$
$$M^{(2)} = \beta\left[\left(\frac{4}{n} - 1\right) - 2m\alpha' + (\beta^2 - 3\alpha'^2)\right] \tag{C10}$$

and $M^{(3)}$ and $M^{(4)}$ are the same as $M^{(1)}$ and $M^{(2)}$, except that α' is replaced by α''. As expressed in (31), eqs (C4) to (C9) can be arranged in the 6×6 matrix, $\mathbf{M}$, multiplied by a vector $\mathbf{C}$ that contains the undetermined coefficients A to F. As discussed in the text, the solution to $\det(\mathbf{M}) = 0$ gives an expression for q' as a function of k'.

For exponentially varying viscosity in two adjoining half-spaces, we must prevent divergence of W for both $z > 0$ and $z < 0$. Thus, we require $A = B = G = H = 0$. We need only four boundary conditions to determine the four remaining unknowns. Eqs (C6) to (C9) then form the rows of the 4×4 matrix, $\mathbf{M}$, times the coefficient vector $\mathbf{C}$.

For the case of linearly decreasing density with depth, we need to solve (44). For the upper half-space, we use (46) and

(47). For the lower half-space, we use the solution:

$$W_2 = E\,e^{kz} + Fkz\,e^{kz}. \tag{C11}$$

After some simplification, boundary conditions like those in (C4) to (C9) become

$$A\,e^{ks_1} + B\,e^{-ks_1} + C\,e^{ks_2} + D\,e^{-ks_2} = 0, \tag{C12}$$

$$As_1\,e^{ks_1} - Bs_1\,e^{-ks_1} + Cs_2\,e^{ks_2} - Ds_2\,e^{-ks_2} = 0, \tag{C13}$$

$$A + B + C + D - E = 0, \tag{C14}$$

$$As_1 - Bs_1 + Cs_2 - Ds_2 - E - F = 0, \tag{C15}$$

$$A\mu_1(2+\delta) + B\mu_1(2+\delta) + C\mu_1(2-\delta) + D\mu_1(2-\delta) - 2E\mu_2 - 2F\mu_2 = 0, \tag{C16}$$

$$-A\mu_1 s_1\delta + B\mu_1 s_1\delta + C\mu_1 s_2\delta - D\mu_1 s_2\delta + 2E(\mu_1 - \mu_2) - 2F\mu_1 = 0, \tag{C17}$$

where s_1, s_2, and δ are defined by (47). As before, eqs (C12) to (C17) form a 6×6 matrix, **M**, which must satisfy $\det(\mathbf{M}) = 0$.